

Relaxed but Highly Compact Diansa Metallacyclophanes

Pau Farràs,[†] Francesc Teixidor,[†] Isabel Rojo,[†] Raikko Kivekäs,[‡] Reijo Sillanpää,[§] Patricia González-Cardoso,[†] and Clara Viñas^{*,†}

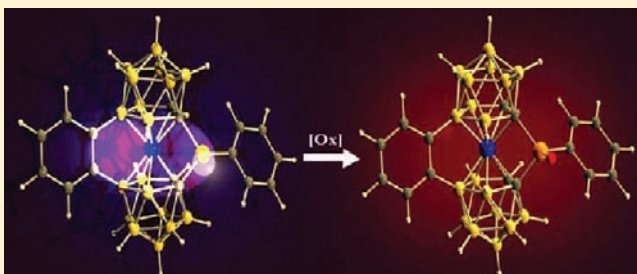
[†]Institut de Ciència de Materials de Barcelona (ICMAB-CSIC), Campus de la U.A.B., E-08193 Bellaterra, Spain

[‡]Department of Chemistry, P.O. Box 55, University of Helsinki, FIN-00014, Finland

[§]Department of Chemistry, University of Jyväskylä, FIN-40351, Finland

S Supporting Information

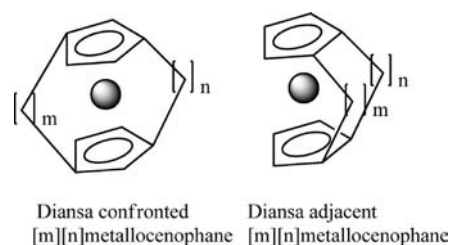
ABSTRACT: A series of monoansa [μ -1,1'-PR-3,3'-Co(1,2-C₂B₉H₁₀)₂]⁻ and diansa [8,8'- μ -(1'',2''-benzene)- μ -1,1'-PR-3,3'-Co(1,2-C₂B₉H₉)₂]⁻ (R = Ph, ^tBu) cobaltabisdicarbollidephanes have been synthesized, characterized and studied by NMR, MALDI-TOF-MS, UV-visible spectroscopy, cyclic voltammetry, and DFT calculations. Single crystal X-ray diffraction revealed a highly relaxed structure characterized by the title angle α of 3.8° ([7]⁻), this being the smallest angle α for a metallacyclophane. In such compounds, the metal-to-phosphorus distance is less than the sum of their van der Waals radii. The availability of a phosphorus lone pair causes an electron delocalization through the metal, as shown by the abnormal ³¹P NMR chemical shift. Remarkably, the combination of a phosphine donor and a phenyl acceptor moieties causes a synergistic effect that is observed through the different techniques used in this study. The importance of having an available lone pair is demonstrated by the oxidation of phosphorus with hydrogen peroxide, sulfur, and elemental black selenium to produce the corresponding P^V compounds. When the electron lone pair is used to form the bond with the corresponding chalcogen atom, the communication between the donor and acceptor moieties on the diansa metallacyclophane is shut down.



INTRODUCTION

The first examples of sandwich metallocarboranes were prepared 46 years ago by Hawthorne et al. using the dicarbollide ion, [C₂B₉H₁₁]²⁻, as a ligand to form *closo* [M(C₂B₉H₁₁)₂]⁻ (M = Co, Fe) icosahedral clusters.¹ The [C₂B₉H₁₁]²⁻ ligand has been compared to [C₅H₅]⁻, as both behave as formal 6-electron donors² to metal atoms via η^5 -face bonding. On the other hand, metallocenes have emerged as the most important organometallic compounds to be systematically developed and studied due to their interesting structures, bonding, electrochemical, and electronic properties that facilitate a plethora of applications.³ The first strained ferrocenophane with a C₂Me₄ bridge, monoansa C₂Me₄[2]ferrocenophane, was reported in 1960,⁴ while a more strained one with a single Si atom bridge was synthesized in 1975.⁵ Later, other related single atom bridging compounds with main group elements and transition group metals (bridging atom X = B, Ge, P, As, S, Se, Al, Ga, Sn, Ni, Mn, Ti, Zr, Hf), monoansa X[1]ferrocenophanes have been reported.⁶ The single atom ansa causes high strain to the original structure of ferrocene, *fc*; therefore, if a second ansa was targeted, this either was adjacent or a multiple atom ansa was required to produce a confronted diansa ferrocenophane. See Chart 1 to visualize the two indicated types of diansa ferrocenophanes: the adjacent and the confronted. We have coined the confronting diansa term to indicate a metallocene with a maximum separation between the two entities, so that one faces the other. Therefore, due to the strain originated by a single atom bridge in a monoansa X[1]ferrocenophane, no example has been published of a fully

Chart 1. - Schematic Representation of Diansa Confronted and Diansa Adjacent Metallocenophanes

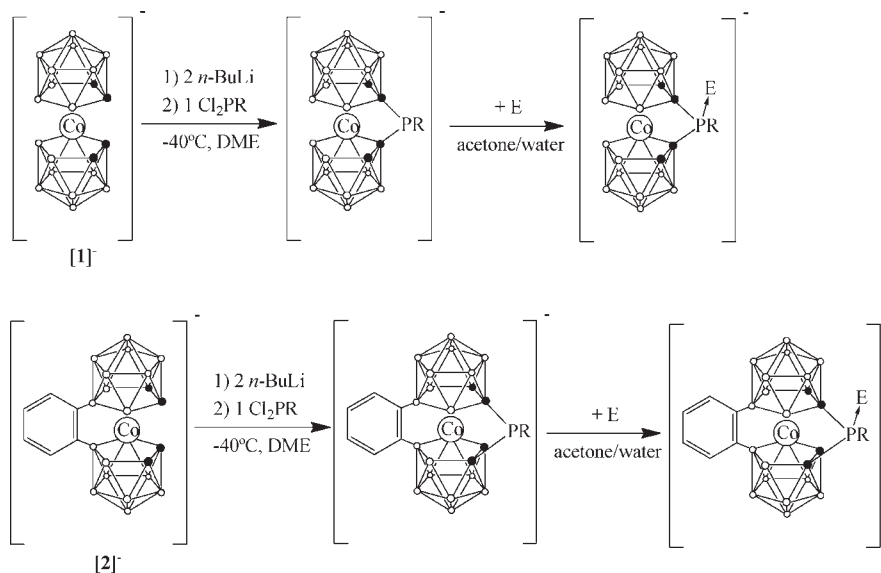


compact confronted diansa ferrocenophane. The most compact confronted ferrocenophane to date is Me₄C₂fcS₃ that can also be written as Me₄C₂[2]S₃[3]ferrocenophane⁷ to indicate the length of the two different ansas.

Cobaltabisdicarbollide, [3,3'-Co(1,2-C₂B₉H₁₁)₂]⁻, [1]⁻, is analogous to the cobaltocenium ion, [Co(C₅H₅)₂]⁺, and like the latter, it demonstrates a simple reversible Co^{3+/2+} couple in electrolyte solutions of organic solvents with a significant cathodic shift of the Co^{3+/2+} reduction potential (-1.80 V (cobaltabisdicarbollide)⁸ vs -1.33 V (cobaltocene),⁹ both taking ferrocene as a reference). While the derivative chemistry of metallocenes has been widely studied, the one of [1]⁻ remains very much unexplored.¹⁰ The fundamental reason for this is the synthetic strategy leading to

Received: June 27, 2011

Published: September 09, 2011

Scheme 1. Synthetic Procedure for the Preparation of Bridged-Phosphorus Derivatives of [1][−] and [2][−]

their derivatives. Two basic substitutions may occur on $[3,3'\text{-Co}(1,2\text{-C}_2\text{B}_9\text{H}_{11})_2]^-$, either on carbon or on boron. With few exceptions,¹¹ substitutions on carbon have been achieved only at an early stage of the synthetic process, that is, on the starting *o*-carborane,¹² but not by direct reaction at the $[3,3'\text{-Co}(1,2\text{-C}_2\text{B}_9\text{H}_{11})_2]^-$ cage. Substitution at boron has been accomplished under Friedel–Crafts conditions,¹³ Kumada^{8,14} and Heck¹⁵ reactions, or with strong alkylating agents.^{2a,14a,16}

The structurally and coordinately similar $[\text{C}_2\text{B}_9\text{H}_{11}]^{2-}$ and $[\text{C}_5\text{H}_5]^-$ ligands differ in their charges, which influences their capacity to stabilize high oxidation states^{2a} and the out of plane disposition of the open face substituents.¹⁷

Our aim in presenting this work has been the synthesis of relaxed monoansa phospho[1]cobaltabisdicarbollidephanes as well as the first example of a relaxed and highly compact diansa metalocenophane: the diansa phospho[1]benzene[2]cobaltabisdicarbollidephanes, in order to establish possible interactions between the P atom bridge and its available lone pair from an ansa and the metal of the metallacyclopentane modulated by a confronting second ansa. It was expected that this confronting two ansa system could tune the structural, electronic, and electrochemical properties of the complex. Oxidation of the bridging P to prevent the P lone pair availability within the metalocycle, by using hydrogen peroxide, sulfur, and selenium, has also been carried on to bring extra information on the $\text{P}\cdots\text{M}$ interaction. To gain further insight into the nature of the latter $\text{P}\cdots\text{M}$ interaction, computational studies on nonoxidized and oxidized monoansa and diansa cobaltabisdicarbollidephanes have been performed. Moreover, the first crystal structure of a compact confronting diansa metalocenophane is reported.

RESULTS

1. Synthesis of Mono and Diasa Cobaltabisdicarbollidephane anions. The targeted anionic bridged phosphine compounds, monoansa ($[3]^-$, $[11]^-$) phospho[1]cobaltabisdicarbollidephanes and diansa ($[7]^-$, $[15]^-$) phospho[1]benzene[2]cobaltabisdicarbollidephanes, are conveniently prepared by metalation of $\text{Cs}[3,3'\text{-Co}(1,2\text{-C}_2\text{B}_9\text{H}_{11})_2]$, $\text{Cs}[1]$, or $\text{Cs}[8,8'-(1'',2''\text{-C}_6\text{H}_4)\text{-}3,3'\text{-Co}(1,2\text{-C}_2\text{B}_9\text{H}_{10})_2]$, $\text{Cs}[2]$,

with 2 equiv of *n*-BuLi, followed by simple reaction with the corresponding dichlorophosphine in 1,2-dimethoxyethane (DME) at low temperature, as shown in Scheme 1. Chart 2 displays the numbering of mono and diansa phospho[1]cobaltabisdicarbollidephane anions synthesized in this paper. The $[\text{NMe}_4]^+$ salts can be produced by metathesis dissolving Li^+ salts in ethanol and adding an aqueous solution of $[\text{NMe}_4]^+\text{Cl}$. Solids corresponding to $[\text{NMe}_4]^+$ salts separate well and can be collected by filtration. Column chromatography is needed to purify the compounds by using a dichloromethane/acetonitrile mixture (70/30). Yields are in the range 51–71%.

The monoansa phospho[1]cobaltabisdicarbollidephane and diansa phospho[1]benzene[2]cobaltabisdicarbollidephane anions may exist at least in four structural/spatial isomers: *meso*, mixed, and racemic mixture, respectively (Figures 1 and 2). Each of these isomers converts into two when the inversion at P is contemplated. Therefore, two *meso*, two mixed, and two racemic mixtures could be generated. The isomers resulting from P inversion need to be accounted for because typical inversion barriers for tertiary phosphines are in the range 28–36 $\text{kcal}\cdot\text{mol}^{-1}$.

All monoansa and diansa cobaltabisdicarbollidephane mixtures were characterized by elemental analysis (EA), IR, MALDI-TOF-MS, ^1H , $^{13}\text{C}\{^1\text{H}\}$, $^{31}\text{P}\{^1\text{H}\}$, and ^{11}B NMR spectroscopies. The combination of these techniques has been very valuable to characterize the structures shown in Chart 2. MALDI-TOF-MS and EA have provided the constitutional purity of the compounds, whereas NMR spectra have provided information about the geometrical isomers present. In this regard, and as an example, Figure S1 in the Supporting Information shows the experimental and calculated patterns for the molecular ion peak of anion $[3]^-$. The IR spectra of all compounds present typical $\nu(\text{B}-\text{H})$ strong bands for *closo* clusters between 2554 and 2577 cm^{-1} .

More information on the isomeric composition could be drawn from the experimental $^{11}\text{B}\{^1\text{H}\}$ NMR spectra for anions $[3]^-$ and $[7]^-$ that are on display in Figures 3 and 4. There it can be seen that there are a larger number of resonances in the range $\delta = +8.3$ to -22.7 ppm for $[3]^-$ and $[7]^-$ with respect to their precursors $[1]^-$ and $[2]^-$. This implies that at least two geometrical isomers are present in solution. The two low-field resonances for $[7]^-$ in

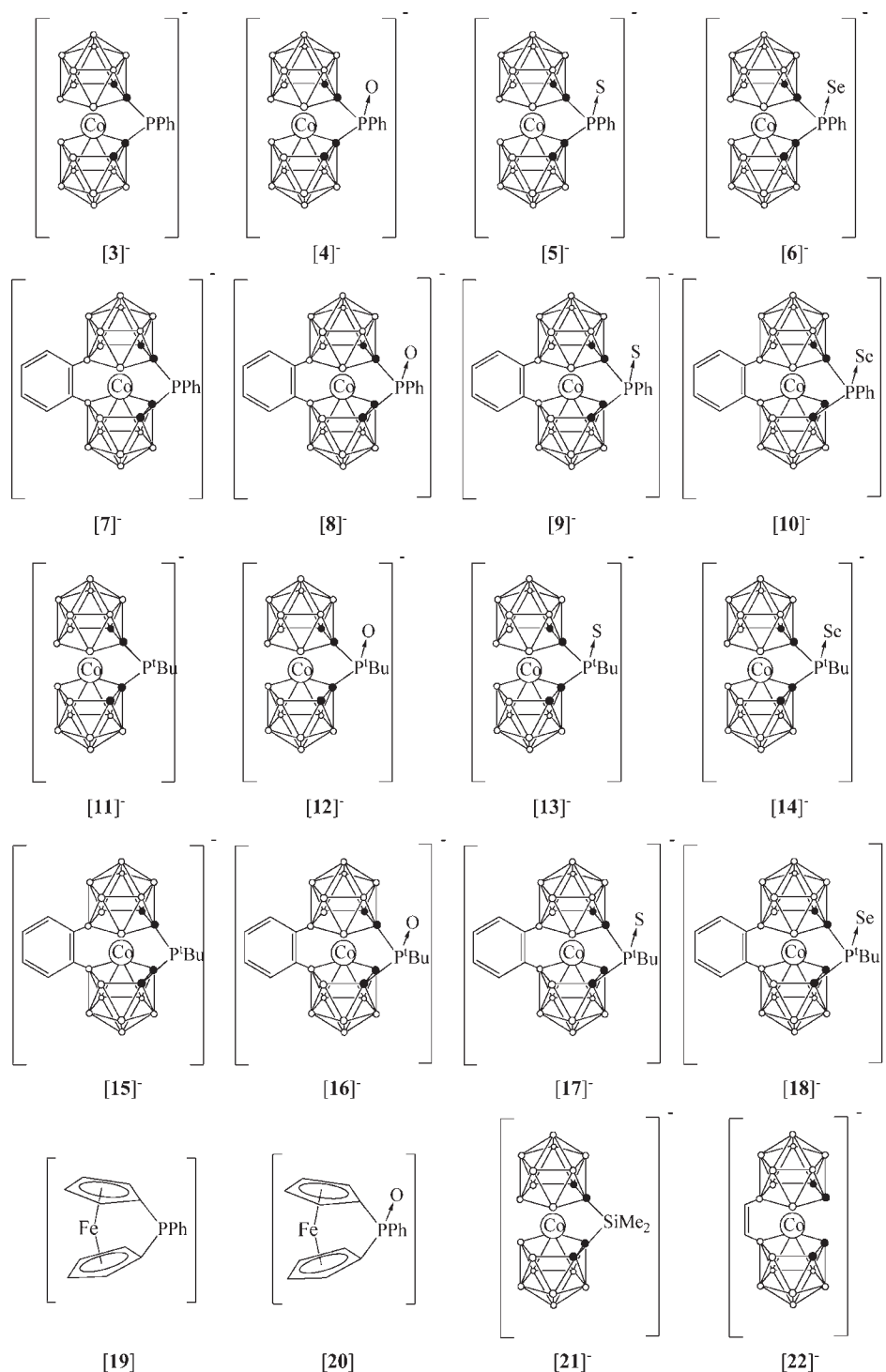
Chart 2. Schematic Drawings of Monoansa and Dianasa $[3]^-$ – $[18]^-$ Anions with Reference Compounds $[19]^-$ – $[22]^-$ 

Figure 4 (top) do not split in the ^{11}B NMR spectrum and, by comparison with the ^{11}B NMR of $[2]^-$, have to be attributed to the B(8)/B(8') atoms bonded to the benzene bridging group. The different intensities of the two low field resonances in $[7]^-$ (Figure 4, middle) are consistent with the coexistence of two isomers as it is in the $^{31}\text{P}\{^1\text{H}\}$ NMR spectra of $[3]^-$, $[7]^-$, $[11]^-$, and $[15]^-$ with two resonances each (see Table 1). The ^1H NMR spectrum of $[3]^-$ displays a group of resonances between $\delta = 7.64$ and 7.48 ppm corresponding to the aromatic hydrogen atoms and

two sets of broad singlets, one at $\delta = 5.70, 5.30$ ppm and the second at $\delta = 4.59, 4.41$ ppm with a ratio 11:2 corresponding to the $\text{C}_c\text{-H}$ hydrogen atoms ($\text{C}_c =$ cluster carbon atom). The presence of two sets of resonances was also in agreement with the presence of two isomers. Finally, the $^{13}\text{C}\{^1\text{H}\}$ NMR spectrum of $[3]^-$ also shows the resonances of the two isomers. The fact that all this variety of techniques has given indication of only two isomers seems to suggest that with high probability only two isomers coexist in solution. An X-ray diffraction study of $[\text{NMe}_4][7]^-$

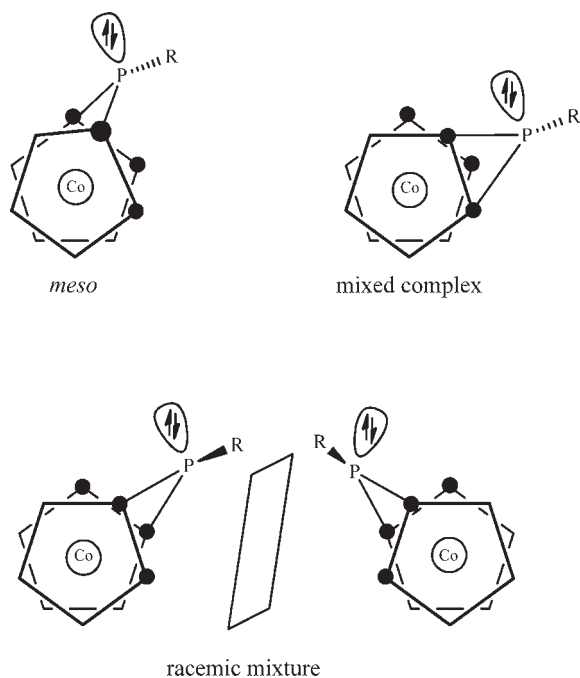


Figure 1. Geometric isomers of the anionic monoansa metallacyclopolyphosphanes $[3]^-$ and $[11]^-$ (view from the top of the pentagonal faces).

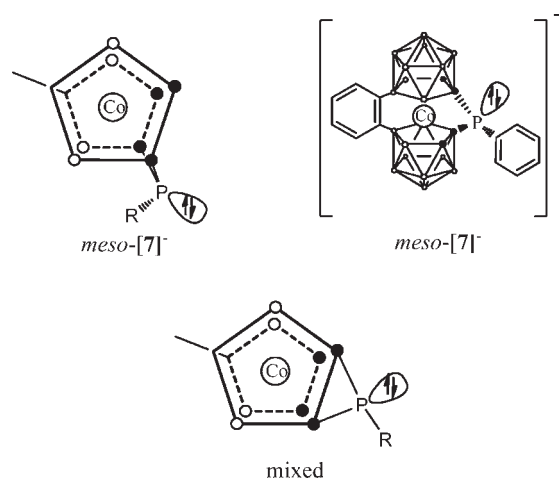


Figure 2. Geometric isomers of the anionic diansa metallacyclopolyphosphanes $[7]^-$ and $[15]^-$ (view from the top of the pentagonal faces).

confirmed that one of the synthesized geometrical isomers was indeed the *meso* form.

1.1. Crystal Structure of $[NMe_4][7]$. Crystals of $[NMe_4][7]$ suitable for an X-ray diffraction study were obtained by slow evaporation of the solvent from a solution of the compound in dichloromethane. The crystals have the formula $[NMe_4][7] \cdot 0.8CH_2Cl_2$. In solid state (space group $P2_1/c$), the structure consists of well-separated $[NMe_4]^+$ cations, diansa cobaltabisdicarbollidephane $[7]^-$ anions, and dichloromethane molecules. The $[7]^-$ anions (two rotamers at the same position in a ratio of 4:1) are disordered. If the major rotamer **a** (the atoms labeled with an **a** affix represent the main rotamer) is present, then a dichloromethane molecule is also present. Figure 5a shows a drawing of such a situation. Figure 5b shows the situation when rotamer **b** is in the asymmetric unit. In such case, dichloromethane

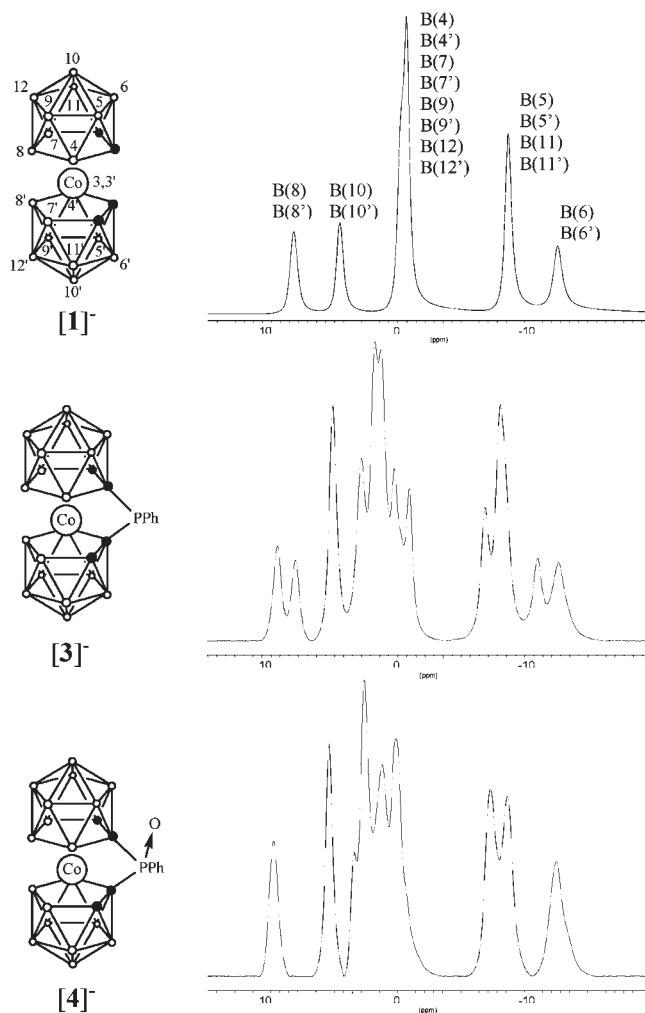


Figure 3. Experimental $^{11}B\{^1H\}$ NMR spectrum of $Cs[1]^-$ (top), $[N(CH_3)_4][3]^-$ (middle), and $[N(CH_3)_4][4]^-$ (bottom).

is not present as the $P1b \cdots C1$ distance is 2.877(7) Å. Figure 5c shows the asymmetric unit as a whole. In rotamer **a**, disordered $[7]^-$ anions show reasonable geometrical parameters, the $Co3 \cdots P1a$ distance is 2.769(1) Å, which is longer than the covalent radii of Co and P (2.30 Å) but much shorter than the sum of van der Waals radii of the atoms (3.80 Å). The cage bridging distances, $C1-P1a$ and $C1'-P1a$ are 1.863(4)° and 1.915(4)°, respectively. The bridging angle, $C1-P1a-C1'$ is 92.6(2)°, is distorted from ideal tetrahedral angle (109.5°) due to the bond to the rigid boron cages.

As expected, the metal in $[7]^-$ is sandwiched by the pentagonal faces of the two dicarbollide units. The pentagonal faces have a mirror conformation, with the torsion angle $C1-c_c-c'_c-C1'$ being 0.88° (c_c = the centroid of C1, C2, B7, B8, B4 face; c'_c = the centroid of C1', C2', B7', B8', B4' face). Thus, the dicarbollide moieties have a *meso* disposition as was observed with the silicon monoansa compound $[1,1'-SiMe_2-3,3'-Co(1,2-C_2B_9H_{10})_2]^-$, $[21]^-$.^{11b}

2. Synthesis of the Mono and Dianza Cobaltabisdicarbollidephane Oxidized Anions with Oxygen, Sulfur, and Selenium. The reasonable stability of these monoansa phosphatocobaltabisdicarbollidephane ($[3]^-$, $[11]^-$) and diansa phosphatocobaltabisdicarbollidephane ($[7]^-$, $[15]^-$) compounds under air has required the use of hydrogen peroxide in acetone at room temperature or sulfur or selenium in refluxing

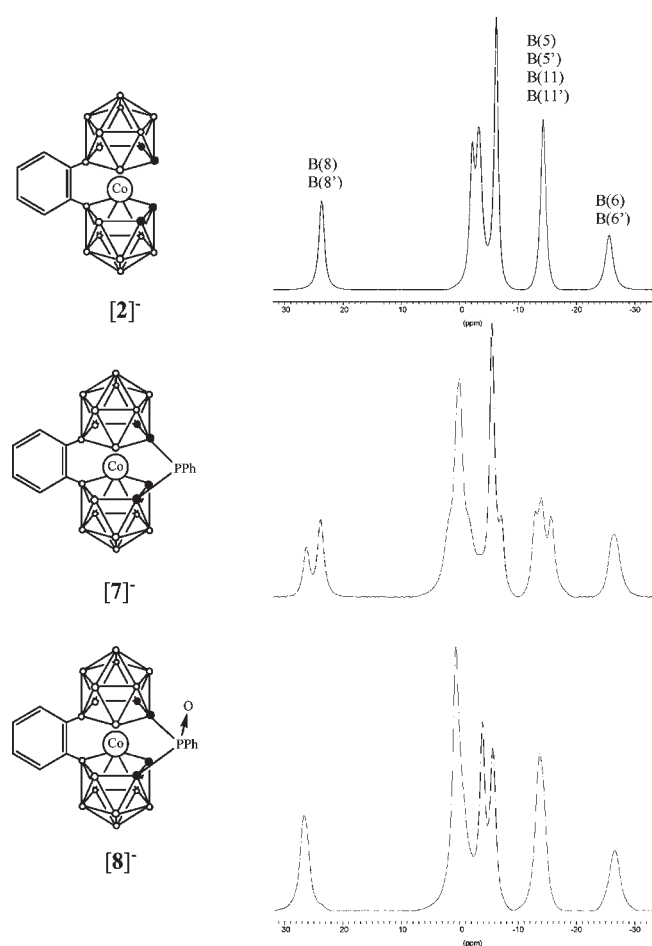


Figure 4. Experimental $^{11}\text{B}\{^1\text{H}\}$ NMR spectrum of $\text{Cs}[2]^-$ (top), $[\text{N}(\text{CH}_3)_4][7]^-$ (middle), and $[\text{NMe}_4][8]^-$ (bottom).

acetone for 30 h to be oxidized to their corresponding monoansa phospho(E)[1]cobaltabisdicarbollidephanes, $[4]^-$, $[5]^-$, $[6]^-$, $[12]^-$, $[13]^-$, and $[14]^-$, and diansa phospho(E)[1]benzene-[2]cobaltabisdicarbollidephane, $[8]^-$, $[9]^-$, $[10]^-$, $[16]^-$, $[17]^-$, and $[18]^-$, (E = O, S, Se). After workup, the compounds were obtained in very good yields (86–97%). Monoansa and diansa phospho[1]cobaltabisdicarbollidephane oxidized species were characterized by EA, IR, MALDI-TOF-MS, ^1H , $^{13}\text{C}\{^1\text{H}\}$, $^{31}\text{P}\{^1\text{H}\}$, and ^{11}B NMR spectroscopies as reported in the Experimental Section in Supporting Information. Strong broad absorptions at $2644\text{--}2550\text{ cm}^{-1}$ due to B–H stretches dominated the IR spectra. P=O, P=S, and P=Se stretches are found as strong and sharp absorptions at $1300\text{--}1205$, $676\text{--}645$, and $701\text{--}688\text{ cm}^{-1}$, respectively. In addition, the IR spectra exhibited strong $\nu(\text{C}\text{--}\text{H})$ stretch absorption at $3050\text{--}3019\text{ cm}^{-1}$ confirming the presence of $\text{C}\text{--}\text{H}$ bonds.

For each of the oxidized species, the *closo* cluster structure was preserved despite changes in the oxidation state from P^{III} to P^{V} . Table 1 shows the $^{31}\text{P}\{^1\text{H}\}$ NMR chemical shift of the oxidized compounds. Most of the resonances appear at a higher field than those corresponding to the phosphine precursors. The shielding capacity on the $^{31}\text{P}\{^1\text{H}\}$ chemical shift followed the tendency $\text{O} > \text{Se} > \text{S}$ (Table 1).

$^{31}\text{P}\{^1\text{H}\}$ NMR spectroscopy corroborated the P oxidation state, the presence of the P–Se bond in $[6]^-$, $[10]^-$, $[14]^-$, and $[18]^-$, and the presence of the two geometrical isomers in the

Table 1. Summary of ^{31}P NMR Resonances of Anions $[3]^-$, $[7]^-$, $[11]^-$, and $[15]^-$ and Their Corresponding Oxidized Compounds

compounds	$\delta^{31}\text{P}$ (ppm)	compounds	$\delta^{31}\text{P}$ (ppm)	$\Delta\delta$ (ppm)	$^1J(^{31}\text{P}, ^{77}\text{Se})$ (Hz)
$[3]^-$	79.1 (15%) 71.1 (85%)	$[4]^-$	35.9 (7%) 33.7 (90%)	−43.2 −37.4	–
		$[5]^-$	73.3 (3%) 71.7 (95%)	−5.8 +0.6	–
		$[6]^-$	73.2 (9%) 69.8 (83%)	−5.9 −1.3	833
$[7]^-$	77.3 (30%) 73.2 (70%)	$[8]^-$	36.2 (33%) 33.5 (67%)	−41.1 −39.7	–
		$[9]^-$	72.9 (30%) 68.3 (70%)	−4.4 −4.9	–
		$[10]^-$	71.0 (30%) 62.7 (70%)	−6.3 −10.5	848
$[11]^-$	88.3 (90%) 81.9 (10%)	$[12]^-$	52.7 (100%)	−35.6	–
		$[13]^-$	95.3 (90%) 92.5 (10%)	+7.0 +10.6	–
		$[14]^-$	98.9 (90%) 94.4 (10%)	+10.6 +12.5	679
$[15]^-$	96.7 (22%) 89.9 (78%)	$[16]^-$	55.2 (50%) 52.2 (50%)	−41.5 −37.7	–
		$[17]^-$	99.9 (20%) 95.2 (80%)	+3.2 +5.3	–
		$[18]^-$	105.0 (10%) 97.5 (90%)	+8.3 +7.6	692

oxidized species. Evidence for the formation of the P–Se bond can be drawn from the $^{31}\text{P}\{^1\text{H}\}$ NMR spectra of the anionic $([\text{Co}(\text{C}_2\text{B}_9)_2])\text{SePR}$ species. Upon prolonged recording times, two satellite lines due to the $^1J(^{31}\text{P}, ^{77}\text{Se})$ appeared, indicating the presence of a P–Se bond. According to the literature, the coupling constants $^1J(^{31}\text{P}, ^{77}\text{Se})$ can reach values ranging from 500 to 1130 Hz for P=Se.¹⁸ A large $^1J(^{31}\text{P}, ^{77}\text{Se})$ value indicates a strong electron withdrawing capacity of the substituents attached to the phosphorus atom,¹⁹ an increased *s*-character for the phosphorus lone pair,²⁰ and a more positive P atom.²¹ The ^{77}Se satellites, $^1J(^{31}\text{P}, ^{77}\text{Se}) = 833, 848, 679,$ and 692 Hz, centered at 69.8, 62.7, 98.9, and 97.5 ppm for compounds $[6]^-$, $[10]^-$, $[14]^-$, and $[18]^-$, confirmed the formation of a P–Se bond. The $^{31}\text{P}\{^1\text{H}\}$ NMR resonances for the monoansa $[6]^-$, $[10]^-$ and diansa $[14]^-$ and $[18]^-$ $([\text{Co}(\text{C}_2\text{B}_9)_2])\text{SePR}$ anionic species appeared at lower field than for Ph_3PSe ($\delta = 35.8$ ppm).²² As shown in Table 1, the coupling constant value $^1J(^{31}\text{P}, ^{77}\text{Se}) = 730$ Hz for Ph_3PSe ²³ is smaller than that for $[6]^-$ and $[10]^-$ but larger than for $[14]^-$ and $[18]^-$ anionic species. Table 1 indicates that the magnitude of the $^1J(^{31}\text{P}, ^{77}\text{Se})$ coupling constant is slightly influenced by the presence of the second ansa (15 Hz), whereas the organic substituent at the phosphorus atom (Ph or ^tBu) produces a considerable tuning (155 Hz).

As discussed, the $^{31}\text{P}\{^1\text{H}\}$ NMR of the oxidized species has clearly shown the coexistence of two isomers in solution, in agreement with the $^{31}\text{P}\{^1\text{H}\}$ and $^{11}\text{B}\{^1\text{H}\}$ NMR of the nonoxidized precursors. This would imply a complicated $^{11}\text{B}\{^1\text{H}\}$ NMR

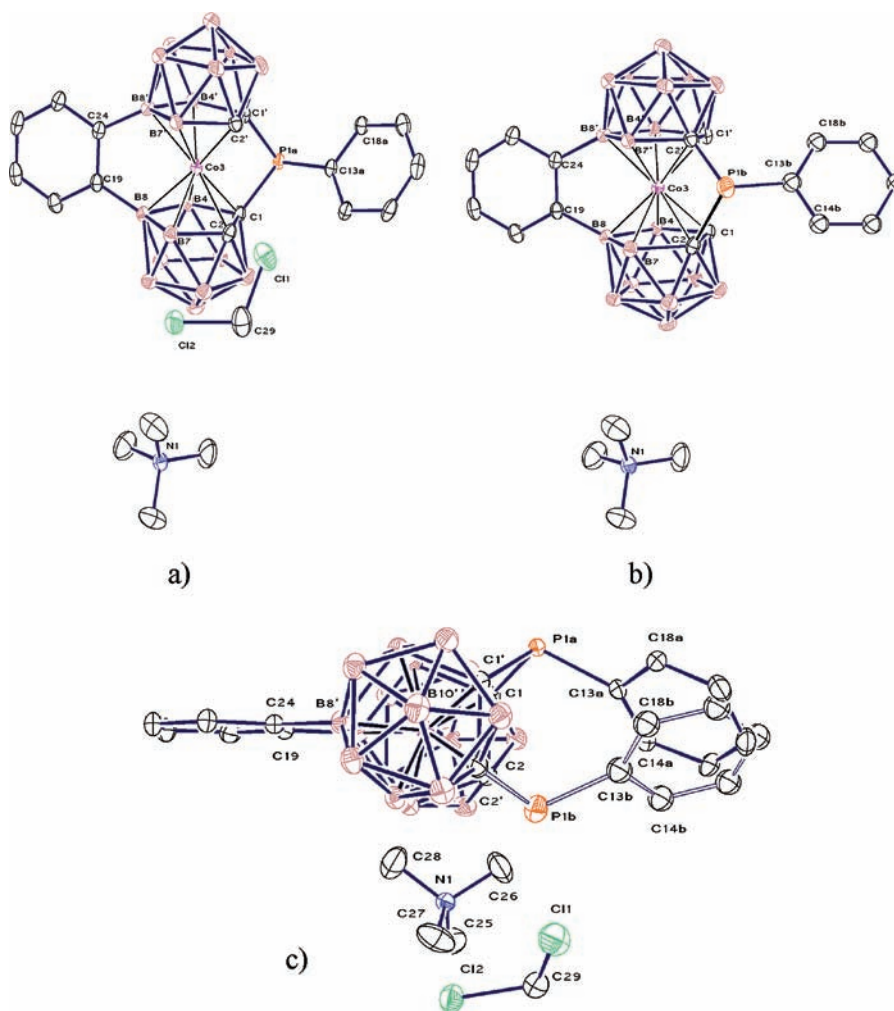


Figure 5. Molecular structure of $[\text{NMe}_4][7] \cdot 0.8\text{CH}_2\text{Cl}_2$. (a) The structure with dichloromethane molecule; (b) the structure without dichloromethane molecule; (c) the top view of the situation in the asymmetric unit (P1a has a population of 0.8 and P1b 0.2). The thermal ellipsoids are set at 30% probability.

that would account for the two oxidized isomers in solution. Surprisingly, this is not the case; the 2:2:1:3:2:2:2:2:2, 2:6:2:2:4:2, or 1:1:4:2:2:4:2 patterns in the range $\delta = +8.6/-22.8$ ppm for the monoansa metallacyclophanes and $\delta = +26.7/-26.6$ ppm for the dianza metallacyclophanes with even fewer resonances than for the monoansa validate a *closo* cluster with unexpectedly coincidental overlap. Figures 3 and 4 display the experimental $^{11}\text{B}\{^1\text{H}\}$ NMR spectra for oxidized anions $[4]^-$ and $[8]^-$.

The ^1H NMR spectra for $[4]^-$, $[5]^-$, and $[6]^-$ display two groups of resonances with a ratio of 2:3, one at 7.68–7.59 ppm and the second at 8.16–8.09 ppm, that correspond to the hydrogen atoms on the phenyl group. The broadness of these resonances is also indicative of at least two isomers in solution. Importantly, the MALDI-TOF-MS of anion $[6]^-$ displays the molecular ion peak at m/z 509.65 and a fragmentation peak at m/z 429.66 corresponding to the loss of H_2Se (Figure S1b).

These techniques have shown the existence of two isomers, but how are they?

2.1. Crystal Structures of $[\text{NMe}_4][4]$, $[\text{NMe}_4][5]$, and $[\text{NMe}_4][6]$. Single crystals suitable for X-ray diffraction studies were grown by slow evaporation of compounds $[\text{NMe}_4][4]$ and $[\text{NMe}_4][5]$ in dichloromethane solutions and by slow evaporation of $[\text{NMe}_4][6]$ in toluene. Table 2 contains the crystal data of the

compounds and Table 3 lists selected bond lengths and angles. All three compounds are formed from $[\text{NMe}_4]^+$ cations and the relevant anions. The space group of $[\text{NMe}_4][4]$ is centrosymmetric ($C2/c$), but for $[\text{NMe}_4][5]$ ($P2_12_12_1$) and $[\text{NMe}_4][6]$ ($P2_1nb$), it is chiral. Compound $[\text{NMe}_4][5]$ was refined as a racemic twin. Figures 6–8 show the structures of the anions: all have a “racemic” conformation. The Co–P distances in all three anions are very close to each other (from 2.767(1) to 2.778(2) Å). For the Co–P distances, a similar discussion is valid as for $[\text{NMe}_4][7]$. The P=E bond lengths (O, S, Se) are 1.476(3), 1.9373(16), and 2.0904(14) Å, respectively. The calculated values using covalent radii by Pyykkö²⁴ are 1.59, 1.96, and 2.09 Å. The measured values compare well with the distances obtained from the covalent radii by Pyykkö, except for the P=O bond, which is much shorter. If the P=O bond is calculated as a triple bond, the value is 1.47. This value is very close to the measured result and comparable to the calculated ones (1.4976 Å for $[4]^-$, 1.4937 Å for $[8]^-$, and 1.5005 Å for $[12]^-$). Other important geometrical parameters are also presented in Table 4. All structural parameters indicate very similar structures for $[4]^-$, $[5]^-$, and $[6]^-$ ions.

The crystal packing of $[\text{NMe}_4][4]$ reveals two weak P–O1...H–C (C19 and C22) hydrogen bonds (the O...H distances are

Table 2. Summary of Crystallographic Data for [NMe₄]⁺ Salts of [4][−]–[7][−]

compound	[NMe ₄][4]	[NMe ₄][5]	[NMe ₄][6]	[NMe ₄][7] · 0.8CH ₂ Cl ₂
Formula	C ₁₄ H ₃₇ B ₁₈ CoNOP	C ₁₄ H ₃₇ B ₁₈ CoNPS	C ₁₄ H ₃₇ B ₁₈ CoNPSe	C _{20.8} H _{40.6} B ₁₈ CoNP
<i>M_r</i>	519.93	535.99	582.89	645.94
<i>T</i> /K	293	173	173	173
Crystal system	monoclinic	orthorhombic	orthorhombic	monoclinic
Spacegroup (no.)	C2/c (15)	P2 ₁ 2 ₁ 2 ₁ (19)	P2 ₁ nb (33)	P2 ₁ /c (14)
<i>a</i> (Å)	21.886(5)	10.6695(4)	10.4360(3)	10.508(3)
<i>b</i> (Å)	13.965(5)	14.5788(6)	11.2927(3)	15.676(3)
<i>c</i> (Å)	18.903(3)	17.5974(6)	23.4638(7)	20.258(7)
<i>α</i> (deg)	90	90	90	90
<i>β</i> (deg)	103.02(2)	90	90	90.323(2)
<i>γ</i> (deg)	90	90	90	90
<i>V</i> (Å ³)	5629(3)	2737.25(18)	2765.22(14)	3336.9(16)
<i>Z</i>	8	4	4	4
<i>D</i> _{calc} (g cm ^{−3})	1.227	1.301	1.400	1.286
<i>μ</i> (Mo K _α) (mm ^{−1})	0.678	0.0771	2.004	0.708
<i>R</i> _{int}	0.019	0.082	0.065	0.056
Used reflections	4961	5208	5968	5840
Parameters	329	330	329	422
<i>R</i> ₁ ^a	0.1151 (0.0505) ^b	0.1035 (0.0542)	0.0993 (0.0530)	0.1471 (0.0635)
<i>wR</i> ₂ ^c	0.1394 (0.1228)	0.1111 (0.0747)	0.1043 (0.0713)	0.1508 (0.0776)
Flack's parameter		0.47(2)		
Largest peak and hole (eÅ ^{−3})	0.470 to −0.320	0.534 to −0.339	0.502 to −0.497	0.776 to −0.534

^a $R_1 = \sum ||F_o| - |F_c|| / \sum |F_o|$. ^b Values in parentheses for reflections with $I > 2.0\sigma(I)$. ^c $wR_2 = \{\sum [w(F_o^2 - F_c^2)^2] / \sum [w(F_o^2)^2]\}^{1/2}$ and $w = 1/[\sigma^2(F_o^2) + (aP)^2 + (bP)]$, where $P = (2F_c^2 + F_o^2)/3$.

2.419 and 2.521 Å, the O···H–C angles are 152 and 148°, respectively). In addition, there are weak B–H···H–C interactions between the CH₃ hydrogens of [NMe₄]⁺ cations and the B–H vertex of the anions to stabilize the structure. The crystal packing of [NMe₄][5] and [NMe₄][6] reveal only the weak B–H···H–C interactions.

DISCUSSION

1. Structural Details. Ferrocenophanes are the paradigm of metallocenophanes; therefore, a structural comparison of the cobaltacyclophanes described in this paper with the equivalent ferrocenophanes is of relevance. In this regard, we have compared the structures of phospho[1]ferrocenophanes and phospho[1]cobaltabisdicarbollidephanes, along with the oxidation products of monoansa phospho[1]cobaltabisdicarbollidephane, [4][−], [5][−], [6][−], and diansa phospho[1]benzene[2]cobaltabisdicarbollidephane [7][−]. The most remarkable structural features as a result of the strain induced by the phospho-bridge are the tilt angle α , that is positive or negative depending on the opening or closure of the C₂B₃ planes around the Co(III) ion ([7][−], −3.8(3)°; [4][−], −9.3(3)°; [5][−], −9.3(2)°; [6][−], −9.5(3)°) and the angles β and β' ([7][−], 44.0 and 44.4°; [4][−], 41.4 and 43.3°; [5][−], 41.5 and 42.6°; [6][−], 40.9 and 41.9°) (Table 4 and Figure 9a). Comparison of the geometrical parameters of these monoansa phospho[1]cobaltabisdicarbollidephane derivatives, [4][−], [5][−], [6][−] with each other reveals their similarity. On the other hand, if the α and β values of [4][−]–[6][−] are compared to the values of the corresponding phospho[1]ferrocenophane^{25,26} derivatives, such as compounds 19 (P^{III}) and 20 (P^V), for which the α values

Table 3. Selected Bond Lengths (Å) and Angles (deg) for the Anions [4][−]–[7][−]

compound	[4] [−]	[5] [−]	[6] [−]	[7] ^{−a}
bond lengths (Å)				
Co(3)–C(1)	2.013(4)	2.017(4)	2.017(5)	2.011(4)
Co(3)–C(1')	2.019(4)	2.013(4)	2.008(6)	1.995(4)
Co(3)–C(2)	2.043(4)	2.037(4)	2.049(5)	2.019(4)
Co(3)–C(2')	2.047(4)	2.052(4)	2.031(6)	2.018(4)
Co(3)–B(8)	2.141(5)	2.135(5)	2.131(7)	2.081(5)
Co(3)–B(8')	2.143(5)	2.134(5)	2.127(6)	2.093(4)
Co(3)–P(1)	2.7668(13)	2.7785(12)	2.7782(15)	2.7687(13)
P(1)–E(1)	1.476(3)	1.9373(16)	2.0904(14)	–
P(1)–C(1)	1.835(4)	1.837(4)	1.819(6)	1.863(4)
P(1)–C(1')	1.844(4)	1.856(4)	1.856(5)	1.915(4)
P(1)–C(13)	1.793(4)	1.802(4)	1.805(5)	1.832(5)
C(1)···C(1')	2.674(6)	2.673(6)	2.658(7)	2.731(6)
C(2)···C(2')	3.887(6)	3.873(7)	3.879(7)	2.896(6)
angles (deg)				
C(1)–Co(3)–C(1')	83.10(16)	83.13(17)	82.7(2)	85.95(16)
C(1)–P(1)–C(1')	93.24(18)	92.75(18)	92.7(2)	92.55(17)
Co(3)–P(1)–E(1)	120.28(14)	123.75(6)	125.26(6)	–
Co(3)–C(1)–P(1)	91.84(17)	92.13(18)	92.7(2)	91.16(17)
Co(3)–C(1')–P(1)	91.36(18)	91.72(19)	91.9(2)	90.15(18)
C2–C1···C1'–C2'	−116.3	−118.0	−115.7	1.3

^a The values in the main component.

are −26.9° and −25.4°, respectively (β values are 32.3° and 34.4°), large differences are found. The α for monoansa

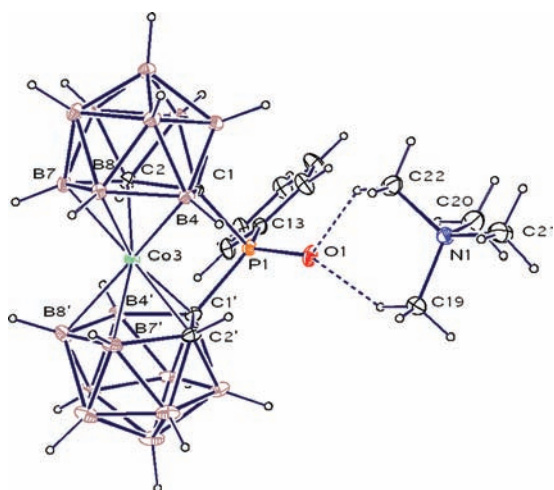


Figure 6. Molecular structure of $[\text{NMe}_4][4]$. The thermal ellipsoids are set at 15% probability.

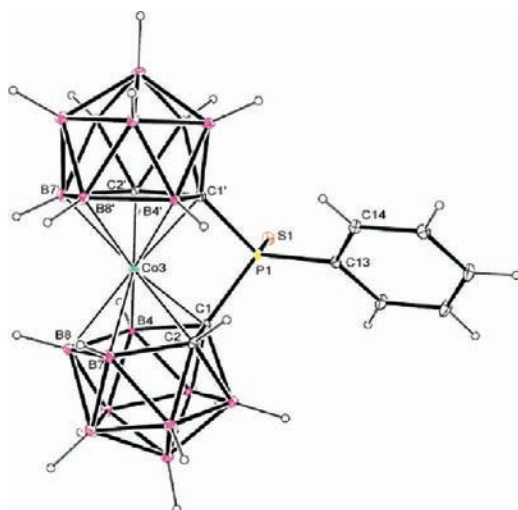


Figure 7. Molecular structure of $[\text{NMe}_4][5]$. The thermal ellipsoids are set at 15% probability. $[\text{NMe}_4]^+$ has been omitted for clarity.

dimethylsilyl[1]cobaltabisdicarbollidephane $[21]^-$ is -6.8° , smaller than that found in $[4]^-$ – $[6]^-$.

As it would be expected, the effect of the chalcogen atom on the phosphorus does not affect significantly the geometrical parameters, only β and β' become slightly smaller as the covalent radius of the chalcogen is bigger. Of importance is the effect of the benzene-bridge in $[2]^-$ as it causes α to be $+6.8^\circ$,^{13b} being among the smallest angles reported to date for monoansa or dianza compounds. This clearly shows the synergistic effect of one ansa to the confronting one. For the monoansa metallocyclophanes ($[4]^-$, $[5]^-$, $[6]^-$) angle α is between -9.3 and -9.5° , while the introduction of the confronting ansa moiety (compound $[7]^-$) causes a relaxation of the structure to an angle α of -3.8° . On the other hand, in aromatic monoansa $[2]^-$ ^{13b} and ethene monoansa $[22]^-$ ²⁷ ions, the C_c – Co (III) distances are longer than in the corresponding dianza $[7]^-$ ion. It is possible then to summarize that a P bridge through C atoms shortens Co – C_c bonds whereas an aromatic monoansa bridge through B atoms elongates Co – C_c bonds. Angle δ is almost 180° for mono and dianza phospho[1]cobaltabisdicarbollidephanes while

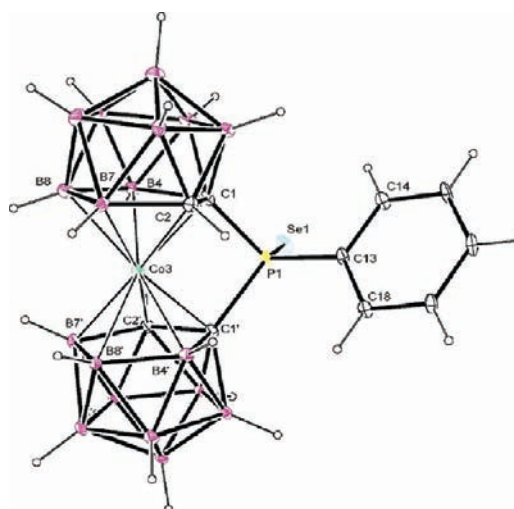


Figure 8. Molecular structure of $[\text{NMe}_4][6]$. The thermal ellipsoids are set at 15% probability. $[\text{NMe}_4]^+$ has been omitted for clarity.

Table 4. Selected Structural Data for the $[\text{NMe}_4]^+$ Salts of the Studied Compounds in Comparison with Phospha[1]ferrocenophanes ($[19]$ and $[20]$)^a

compound	α (deg) ^b	β (deg) ^c	δ (deg)	θ (deg)	$\text{M}\cdots\text{E}$ (Å)
$[1]^{-47}$	+2.0	-	177.6	-	-
$[4]^-$	-9.3(3)	41.4	174.4	93.2(2)	2.767(1)
		43.3			
$[5]^-$	-9.3(2)	41.5	174.8	92.8(2)	2.779(1)
		42.6			
$[6]^-$	-9.5(3)	40.9	174.6	92.7(2)	2.778(2)
		41.9			
19^{25a}	-26.7	32.5	159.8	90.6(3)	2.774(3)
19^{25b}	-26.9	32.3	159.8	90.7(2)	2.774(1)
20^{26}	-25.4(1)	34.4	161.4	94.3(1)	2.7116(7)
$[21]^{-11b}$	-6.8	43.2	175.6	90.4(1)	2.787(1)
$[2]^{-13b}$	+6.8	42.1	174.5	90.3	-
$[22]^{-27}$	+7.1	42.5	174.2	90.2	-
$[7]^{-d}$	-3.8(3)	44.0	177.4	92.6(2)	2.769(1)
		44.4			

^a Also data for ions $[21]^-$, $[2]^-$, and $[22]^-$ are included. ^b The negative value means that the distances between carbon atoms between upper and lower belt have been decreased from the parallel situation (positive value indicates the opposite). ^c Two different values refer to β and β' . ^d Values in the main component.

for phospho[1]ferrocenophane is 160° , much smaller given the higher distortion found on the latter.

Although some computational studies on the phosphorus–chalcogen bond were found in the literature,²⁸ few studies have been done on bulky phosphines or with strongly electron-withdrawing groups bonded to phosphorus.²⁹ The nature of the phosphorus–chalcogen bonds of $[4]^-$ – $[8]^-$ and phospho[1]ferrocenophane derivatives was determined by DFT calculations, natural bond orbital (NBO) analysis, and quantum theory of atoms in molecules (QTAIM). The geometries of these derivatives were modeled by DFT calculations to have the full set of compounds. Previously, we explored the crystallographic entries in the Cambridge Data Base (CSD)³⁰ on monoansa and dianza

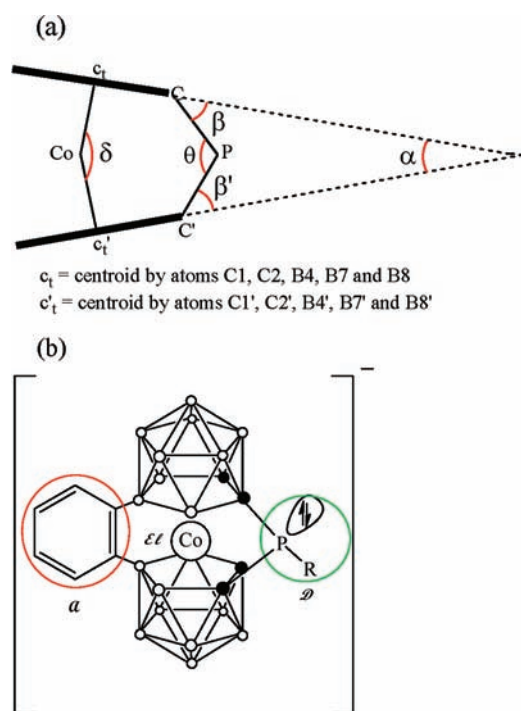


Figure 9. (a) Structural features as a result of the strain induced by the phospho-bridge. (b) Schematic drawing of the dianisa phospho[1]benzene[2]cobaltabisdicarbollidephosphane units. D = donor group; A = acceptor group.

cobaltabisdicarbollide anions that connect the dicarbollide units either through the two C_c atoms, the two B atoms, or hybrid C_c and B atoms. Only a crystal structure (CSD code HOBFI0) of anionic monoansa cobaltabisdicarbollide through the C_c atoms showing a *meso* conformation has been found.^{11b} When exploring the crystallographic entries of anionic monoansa cobaltabisdicarbollide through the B atoms, nine crystal structures showing *meso* conformation have been found.³¹ There is no crystal structure of dianisa cobaltabisdicarbollide reported at the CSD. On the basis of this search and the crystal structures reported in this paper, all theoretical calculations have been done on the *racemic* form for the anionic monoansa phospho[1]cobaltabisdicarbollidephanes and on the *meso* form for the anionic dianisa phospho[1]benzene[2]cobaltabisdicarbollidephanes. The resulting optimized geometries are given in Table 5. The good agreement between the calculated and crystallographic structural data establishes that the calculated compounds provide an accurate model for the geometrical study. It is worth to mention that phosphorus oxidation causes a decrease on α and an increase on β in both ferrocene and cobaltabisdicarbollide moieties. Finally, the dianisa phospho[1]benzene[2]cobaltabisdicarbollidephane is the first reported compound that as a result of having dianisa confronted bridges causes a relaxation of the structure, mostly due to the compensation of both ansa elements, that is, α : +6.0° for [2][−] and −5.8° for [7][−]. Experimental α values are +6.8° for [2][−], and −3.8° for [7][−].

When comparing the structures of phospho[1]ferrocenophanes and phospho[1]cobaltabisdicarbollidephanes, we noticed that the former compounds, 19 and 20, have distorted cyclopentadiene planes shown by the geometrical parameter α (−27.2° and −26.0°, respectively). In contrast, phospho[1]cobaltabisdicarbollidephanes ([3][−]–[6][−]) have less distorted C_2B_3 planes (−10.3° < α <

Table 5. Selected Angles and Distances for the Calculated Compounds in Comparison with Calculated Phospha[1]ferrocenophanes ([19] and [20])^a

compound	α (deg)	β (deg)	δ (deg)	θ (deg)	M···E (Å)
[19]	−27.23	31.46	160.32	89.45	2.812
[20]	−26.03	33.72	161.58	93.28	2.732
[1] [−]	0.00	−	−	−	−
[2] [−]	+6.03	−	−	−	−
[3] [−]	−10.88	40.44	173.87	89.58	2.852
[4] [−]	−10.71	41.32	173.83	91.84	2.809
[5] [−]	−10.35	41.02	174.11	90.97	2.831
[6] [−]	−10.55	41.05	174.35	90.84	2.826
[7] [−]	−5.75	42.00	175.80	90.82	2.811
[8] [−]	−5.76	42.59	175.41	92.66	2.774

^aThe tilt angle α is positive or negative depending on the opening or closure of the C_2B_3 planes around the Co(III) ion.

−10.9°) and this is even more accentuated in the dianisa phospho[1]benzene[2]cobaltabisdicarbollidephane [7][−] and [8][−] where the C_2B_3 planes are almost parallel ($\alpha = -5.8^\circ$). A geometrical consequence of the more pronounced tilting in phospho[1]ferrocenophanes than in phospho[1]cobaltabisdicarbollidephane is that the bridging phosphorus is closer to the sandwiched metal in the latter, even taking into account the relative cobalt and iron van der Waals radii. The crystal structure of [7][−] shows a distance of 2.769(1) Å between Co and P that is smaller than sum of van der Waals radii.³²

To probe the nature of intramolecular interactions, NBO analysis has been performed on anions [3][−]–[8][−]. With the use of the second order perturbation theory analysis included in NBO, it is possible to estimate donor–acceptor interactions between natural bond orbitals, along with their energy. For nonoxidized monoansa [3][−] and dianisa [7][−] anions, three different interactions can be found between phosphorus and cobalt (Figure 10). For [3][−], two of them with an energy of 21 kcal·mol^{−1} correspond to the interactions between the electrons of the P– C_c bonds and the empty 4s orbital on cobalt. The third interaction is found between the lone pair on phosphorus and the same 4s orbital as before, with an energy of 10 kcal·mol^{−1}.

On the other hand, for oxidized anions [4][−], [5][−], and [6][−], there is no interaction between phosphorus and cobalt due to the absence of the P lone pair, which is bonded to the chalcogen atoms (Figure 11). The interactions found in these compounds are between the P– C_c bonds and the empty 4s orbital of cobalt with a similar energy of ca. 8 kcal·mol^{−1} independent of the chalcogen atom. Moreover, it is possible to find interactions of about 12–20 kcal·mol^{−1} between lone pairs on chalcogen and the P– C_c bond, leading to a decrease of the electronic density on the chalcogen. The energy of these interactions follows the tendency O > S > Se. Interactions between the P– C_c bonds and the B6/B6' vertices with an energy of ca. 7 kcal·mol^{−1} have also been observed. These interactions provide extra ways to give electronic density back to the metallacarborane cluster (see Table S1 in Supporting Information for more details).

Finally, in order to prove the existence of a direct interaction between the Co and the P, an AIM (atoms in molecules) analysis on anions [3][−] and [4][−] was performed.³³ A critical point (3, +1) was identified between the Co and the P atoms in both anions indicating the center of a ring rather than the existence of a direct interaction. Figure 10b shows a 2D representation of the

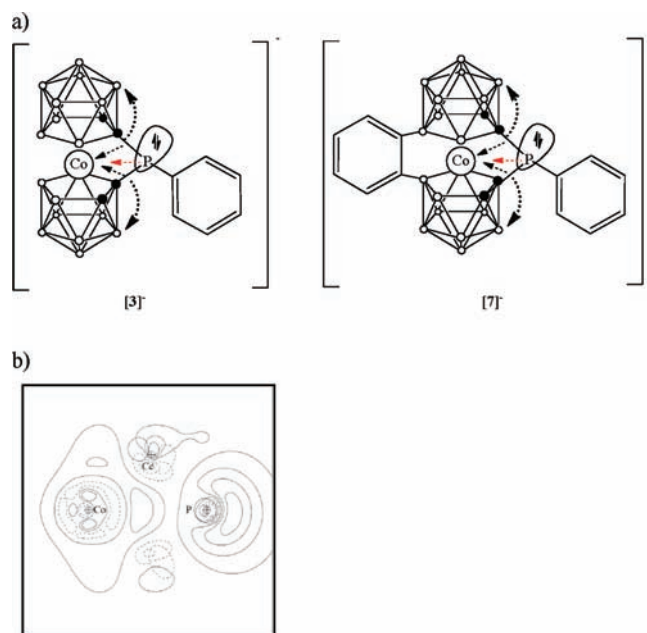


Figure 10. (a) Graphical representation of the interactions found in monoansa [3]⁻ and diansa [7]⁻ anions. (b) 2D plot of the NBO orbitals of monoansa [3]⁻ corresponding to the interaction P–Co. The plane contains Co1–C2–P3 atoms.

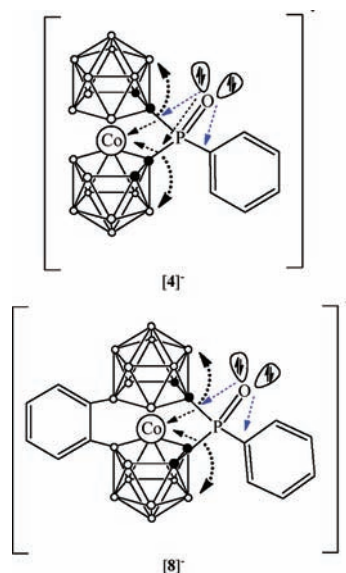


Figure 11. Graphical representation of the interactions found in the oxidized monoansa [4]⁻ and diansa [8]⁻ anions.

NBO orbitals' interaction between phosphorus and cobalt for [3]⁻. Although the analysis has not led to the identification of a dative interaction (BCP), the existence of a critical ring point (RCP in this case) brought us to the hypothesis that the influence of the ansa is found on the metal center, and that this can happen on both sides of the metal, causing a synergistic effect of the diansa observed in the spectroscopic and electrochemical parameters as will be discussed in the next sections.

2. NMR Spectral Considerations. NMR spectroscopy has been a useful tool for the characterization of boranes, carboranes,

and metallacarborane clusters for many years.³⁴ The sensitivity of the electron distribution in carboranes to the presence of substituents has long been apparent.³⁵ However, only few computational analyses of the ¹¹B NMR chemical shifts for metallabisdicarbollide³⁶ and its derivatives^{11b} have been reported and none on ³¹P NMR of phosphines containing metallabisdicarbollide groups. With the aim to obtain an interpretation of the experimental ¹¹B NMR and ³¹P spectra of these monoansa phospho[1]cobaltabisdicarbollidephane and diansa phospho[1]benzene[2]cobaltabisdicarbollidephane species, theoretical calculations of $\delta(^{11}\text{B})$ and $\delta(^{31}\text{P})$ values have been carried out on several of the metallabisdicarbollide derivatives reported in this paper.

2.1. Comparison between ³¹P NMR Spectra of Nonoxidized and Oxidized Species. In the majority of common ligands, the phosphinechalcogenide unit gives a signal to lower field than the parent phosphine.³⁷ In fact, this behavior is common in most phosphine molecules and it is interpreted to be due to an electron donation from phosphorus to chalcogen, causing a decrease in the electron density of the P. It is noticeable (Table 1) that the resonances of the P^{III} anions [3]⁻, [7]⁻, [11]⁻, and [15]⁻ appear at a very downfield chemical shift when compared with the anionic diphosphine [1,1'-(PPh₂)₂-3,3'-Co(1,2-C₂B₉H₁₀)₂]⁻ previously reported by our group that showed resonances at 25 ppm.^{38,29} This means that the electronic environment on phosphorus in the monoansa phospho[1]cobaltabisdicarbollidephanes or diansa phospho[1]benzene[2]cobaltabisdicarbollidephanes is remarkably different, suggesting that electron density from phosphorus is being shared with other parts in the molecule. In addition, once oxidized by chalcogenides (O, S and Se), most of the resonances appear at a higher field than these corresponding to the phosphine precursor (see Table 1). What is responsible for this behavior?

It is known that *o*-carborane cluster is electron-withdrawing through the carbon atoms and, consequently, can deplete electron density on phosphorus.³⁹ This should influence the ³¹P chemical shift of the P atom ansa bonded to cobaltabisdicarbollide via the cluster carbon atoms; however, no "abnormal" ³¹P NMR were observed in our previously reported [1,1'-(PR₂)₂-3,3'-Co(C₂B₉H₁₀)₂]⁻ phosphine derivatives.³⁸ Therefore, the "abnormal" ³¹P NMR observed in monoansa phospho[1]cobaltabisdicarbollidephane and diansa phospho[1]benzene[2]cobaltabisdicarbollidephane has to be attributed to the small cycle generated and/or to the closeness of the Co via a Ligand-to-Metal Charge Transfer (LMCT). In the case of [n]ferrocenophanes, the ⁵⁷Fe Mössbauer spectra suggested the possibility of a dative interaction between the ansa element and the iron atom.^{40,41} This had been observed for phosphorus, carbon, silicon, among others, even though the Fe···X distance was longer than the sum of the covalent radii,^{28d} but shorter than the sum of the van der Waals radii.³²

To interpret the "abnormal" ³¹P NMR chemical shifts, the geometry optimizations indicated in the Structural Details section have been used. Then, a theoretical calculation of ³¹P NMR chemical shifts taking PPh₃ as a reference has been made. The good agreement between the calculated and experimental chemical shifts provided a new evidence to prove that the optimized geometry is a good representation of the molecular structure in solution. Table 6 shows the calculated and experimental chemical shifts for compounds [3]⁻–[8]⁻. The trend between computed and experimental values is in good agreement except for [6]⁻ where the relativistic effect of the Se atom can be important. To rule out that the small cycle was the only influence, a

Table 6. Calculated and Experimental ^{31}P NMR Chemical Shifts for Several Monoansa and Diansa Derivatives^a

	calculated δ (^{31}P)	experimental δ (^{31}P)
$[3]^-$	74.9	71.1
$[4]^-$	19.6	33.7
$[5]^-$	77.6	71.7
$[6]^-$	96.3	69.8
$[7]^-$	78.0	73.2
$[8]^-$	16.9	33.5
μ -P-biphenyl	-6.8	
μ -P(O)-biphenyl	7.8	

^a Two bridge compounds (μ -P-biphenyl and μ -P(O)-biphenyl) without a metal are included as a comparison.

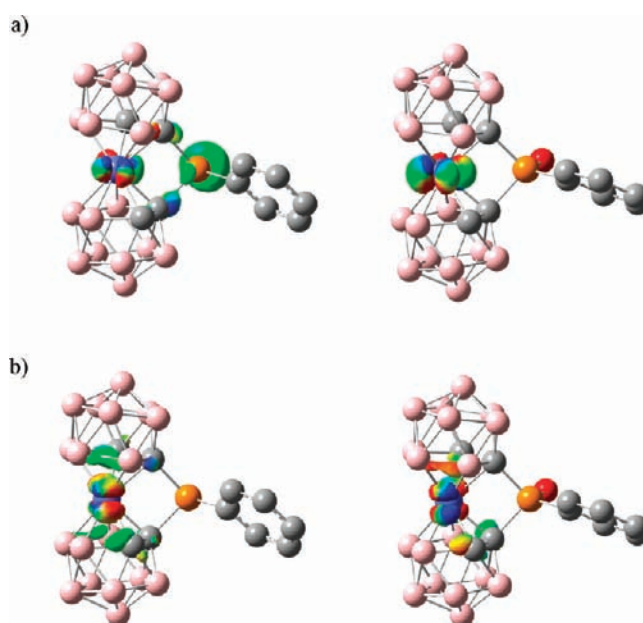
Table 7. Calculated Diamagnetic and Paramagnetic Contributions to the ^{31}P NMR for Several Monoansa and Diansa Derivatives^a

	calc. σ_d δ (^{31}P)	calc. σ_p δ (^{31}P)
$[3]^-$	-701.7	1066.1
$[4]^-$	-702.3	1011.3
$[7]^-$	-694.8	1062.3
$[8]^-$	-696.7	1003.1
μ -P-biphenyl	-684.7	967.4
μ -P(O)-biphenyl	-679.5	976.8

^a Two bridge compounds (μ -P-biphenyl and μ -P(O)-biphenyl) without a metal are included as a comparison.

phospha[1]cobaltabisdicarbollide geometrically similar nonmetal containing rigid cyclophane, μ -P-biphenyl, was computationally studied along with its oxidized form (μ -P(O)-biphenyl). In this case, the calculated ^{31}P NMR chemical shifts follow a "normal" pattern: the oxidized species is more deshielded than the nonoxidized form. Therefore, the presence of a metal center near the phosphorus atom might be responsible for the higher than expected deshielding on the nonoxidized compounds.

These studies were complemented by calculation of the paramagnetic ($\Delta\sigma_p$) and diamagnetic ($\Delta\sigma_d$) contributions to the shielding constant for some oxidized and nonoxidized monoansa and diansa molecules. The results are shown in Table 7. There it may be observed that for the monoansa and diansa metallacyclophanes ($[3]^-$, $[4]^-$, $[7]^-$, and $[8]^-$) the $\Delta\sigma_d$ contribution has almost the same value for nonoxidized and oxidized species. Therefore, the $\Delta\sigma_p$ must be the major contribution responsible for the ^{31}P NMR chemical shift. On the other hand, in the geometrically similar nonmetal containing μ -P-biphenyl, the chemical shift is caused by both $\Delta(\sigma_d)$ that is 5.2 ppm and $\Delta(\sigma_p)$ that is 9.4 ppm. The diamagnetic contribution is mainly attributed to the electron density on the nucleus and this seems to be the same for monoansa $[3]^-$ and $[4]^-$ anions. Conversely, paramagnetic contribution is attributed to electron spins and to the interaction between occupied and unoccupied levels, respectively.⁴² The rather large contribution of the lone pair on phosphorus in $[3]^-$ and $[7]^-$ on the highest occupied molecular orbital (HOMO) causes a larger paramagnetic contribution which is not found when those electrons are bonded to the calchogen atom ($[4]^-$ and $[8]^-$), where the HOMO is centered on the metal (Figures 12 and 13).

**Figure 12.** HOMO (a) and LUMO (b) orbitals of monoansa anions $[3]^-$ (left) and $[4]^-$ (right).

Throughout this paper, we emphasize the synergistic effects of the confronting two ansa moieties. The ^{31}P NMR is another example. The experimental ^{31}P NMR of monoansa and diansa cobaltabisdicarbollidephanes are different, for $[3]^-$ is 71.1, whereas for $[7]^-$ is 73.2 ppm. On the contrary, their oxidized forms $[4]^-$ and $[8]^-$ display the ^{31}P NMR almost at the same δ (^{31}P), 33.7 and 33.5 ppm, respectively. This data suggests that when the lone pair on P is available for inner molecular use, there is synergy between the two bridging units. When this lone pair is unavailable for inner use, as is the case when the P is oxidized, the synergy of the two bridging fragments is switched off.

2.2. Qualitative Description of the ^{11}B NMR Spectra Chemical Shift Dependence. To observe the effect of the P^{III} or P^{V} bridge on the δ (^{11}B) as well as on the paramagnetic and diamagnetic contributions to the ^{11}B NMR spectra of monoansa and diansa compounds, theoretical calculations have also been done. Figure 14 displays the calculated $\Delta\delta$ (^{11}B) resonances of $[3]^-$, $[4]^-$, $[7]^-$, and $[8]^-$ taking as references the chemical shifts of parent $[1]^-$ and $[2]^-$ species, respectively. The analysis of calculated δ (^{11}B) shows a different behavior for monoansa or diansa metallacyclophanes. While for the monoansa species, the most affected vertices (B12 and B12') are the ones antipodal to the C_c -PR bonds, for the diansa compounds, the largest difference in chemical shifts is seen on the vertices B7 and B7' at the C_2B_3 face.

The diamagnetic ($\Delta\sigma_d$) and paramagnetic ($\Delta\sigma_p$) contribution to the shielding differences in monoansa $[3]^-$, $[4]^-$ and diansa $[7]^-$, $[8]^-$ as referred to $[1]^-$ and $[2]^-$, respectively, have been calculated (Figures S2 and S3 in the Supporting Information). For monoansa phospha[1]cobaltabisdicarbollide $[3]^-$ and $[4]^-$, the vertices B(12) and B(12') are the most affected by both contributions ($\Delta\sigma_d$ and $\Delta\sigma_p$). However, as they have opposite signs, $\Delta\sigma_p$ is the contribution that affects the resonances on B(12) and B(12') the most. The same explanation is valid for diansa phospha[1]benzene[2]cobaltabisdicarbollide, $[7]^-$ and $[8]^-$.

3. Cyclic Voltammogram Studies. With no debate, the archetype of the metallocenes is ferrocene. Unlike monoansa or diansa ferrocenophanes, that are invariably strained, the

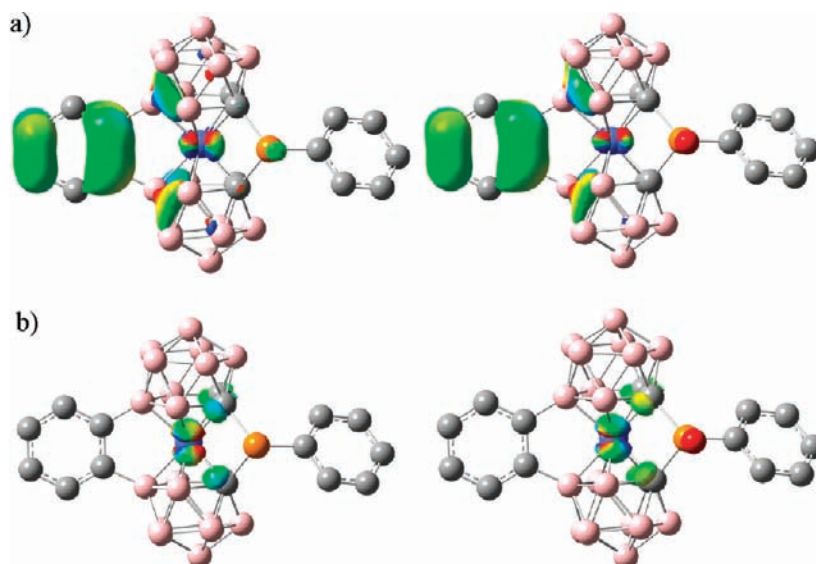


Figure 13. HOMO (a) and LUMO (b) orbitals of diansa anions $[7]^-$ (left) and $[8]^-$ (right).

cobaltabisdicarbollide unit allows for unprecedented and relaxed confronting diansa sandwich complexes without major perturbation of the original sandwich structure as seen at the structural section. Therefore, the peculiar geometric characteristics of cobaltabisdicarbollide has permitted to combine in an unprecedented way a donor, D (the PR bridge), and an acceptor, A (the benzene bridge), in a confronting way (Figure 9b). As a result, $[7]^-$ and $[15]^-$ are highly compact but relaxed phospho[1]-benzene[2]cobaltabisdicarbollidephane species. Indeed, these molecules do not allow for any degree of internal motion, with the possible exception of an inversion on P. No comparable example has been found in the literature for any metallocene, the more compact ones possible being the widely studied diansa-[2,3]ferrocenophanes with both trisulfide (or triselenide) and hydrocarbon bridges.⁷

To examine the effect of the D and A units on the $\text{Co}^{3+/2+}$ couple, the set of cobaltabisdicarbollide anions $[4]^-$, $[5]^-$, $[6]^-$, $[7]^-$, $[8]^-$, $[11]^-$, $[15]^-$, and $[16]^-$ was studied. All CVs of these compounds show one reversible redox wave that corresponds to the $\text{Co}^{3+/2+}$ redox couple, and this is the only wave discussed in this paper to study the influence of the donor and the acceptor bridges. The experimental $E_{1/2}$ values, referenced to f_c , for the $\text{Co}^{3+/2+}$ couple for each anion are indicated in Table 8.

As Lever and co-workers reported,⁴³ an electrochemical parametrization in sandwich complexes of the first row transition metals can be established by assigning electrochemical parameters to the ligands. We will adhere to Lever's approach due to the sandwich nature of the cobaltabisdicarbollide anions. However, certain inaccuracies are expected because Lever's parametrization is generated from data obtained from organic ligands. For metal-centered redox reactions, the following equation is applied:

$$E_{\text{calc}}(M^{n+1}/M^n) = S_M \sum E_L(L) + I_M \quad (1)$$

The parameters S_M and I_M for a particular $M^{n+1/n}$ couple are constants. In organic solvents, for $\text{Co}^{3+/2+}$ they are 0.83(0.05) and $-1.16(0.13)$ V, and for $\text{Fe}^{3+/2+}$, these are 0.99(0.00) and 0.00(0.01) V, respectively, referred to Standard Hydrogen Electrode (SHE).⁴³ Despite the relatively large standard deviation SD, the fact that cobaltabisdicarbollide follows eq 1 derived mostly from metallocenes, indicates that cobaltabisdicarbollide is a

metallocene-like molecule that behaves as such. We have applied eq 1 to calculate the E_L contribution of the ligand $[7,8\text{-C}_2\text{B}_9\text{H}_{11}]^{2-}$ that can be estimated as $-0.00(0.10)$ taken from the experimental $E_{1/2}$ value for $[3,3'\text{-Co-(1,2-C}_2\text{B}_9\text{H}_{11})_2]^-$ obtained in this work. Likewise, E_L for phospho[1]cobaltabisdicarbollidephane $[3]^-$ is $+0.22$ V, whereas for benzene[2]cobaltabisdicarbollidephane $[2]^-$ is -0.35 V.

3.1. The Diansa Phospho[1]benzene[2]cobaltabisdicarbollidephane. Lever parameters have shown the redox ligand additivity in the $\text{Co}^{3+/2+}$ sandwich couple. A possibility existed that the opposing donor influence, D, of the $-\text{PR}$ moiety and the acceptor influence, A, of the bridging benzene could in part cancel themselves. The effect of the benzene bridge was -0.35 V, whereas the bridging PR was $+0.16(0.01)$ V ($R = \text{Ph}$) and $+0.22$ V ($R = \textit{t}\text{Bu}$), both with regard to the parent $[1]^-$. The influence of the R group on monoansa phospho[1]cobaltabisdicarbollidephosphane was almost negligible at this stage. Therefore, a simple addition of both the effect of the acceptor (benzene) and the effect of the donor ($-\text{PR}$), in similarity to Lever's parametrization, would result in a -0.15 V shift. This was, however, not the case and the cooperative result of the synergy of the D and A moieties resulted in a $+0.22$ V shift for $R = \text{Ph}$ or a small -0.05 V shift for $R = \textit{t}\text{Bu}$. Interestingly, the once almost equal R effects ($R = \textit{t}\text{Bu}, \text{Ph}$) in the monoansa phospho[1]cobaltabisdicarbollidephanes become clearly distinct when the D and A synergy is put to work in the diansa phospho[1]benzene[2]cobaltabisdicarbollidephanes. The result of the synergy is not to cancel both effects but to stress the effect of one. For this confronting phospho[1]benzene[2]cobaltabisdicarbollidephane, the anodic shift of the P-R is the enhanced one.

3.1.1. Lowering the Inner Molecular Availability of the Lone Pair on Phosphorus. As the lone pair on P had been considered the basis for its expected D character, its lesser availability anticipated an alteration in the electronic density around the metal core, and therefore, a modified $E_{1/2}(\text{Co}^{3+/2+})$ was predicted. To accomplish this objective, phospho[1]benzene[2]cobaltabisdicarbollidephanes $[7]^-$ and $[15]^-$ were taken to react with hydrogen peroxide and with sulfur to produce covalent P-O bond, compounds $[8]^-$ and $[16]^-$, and P-S bonds, compounds $[9]^-$ and $[17]^-$, respectively. The resulting oxidized molecules either with O or S preserved the original charge of the

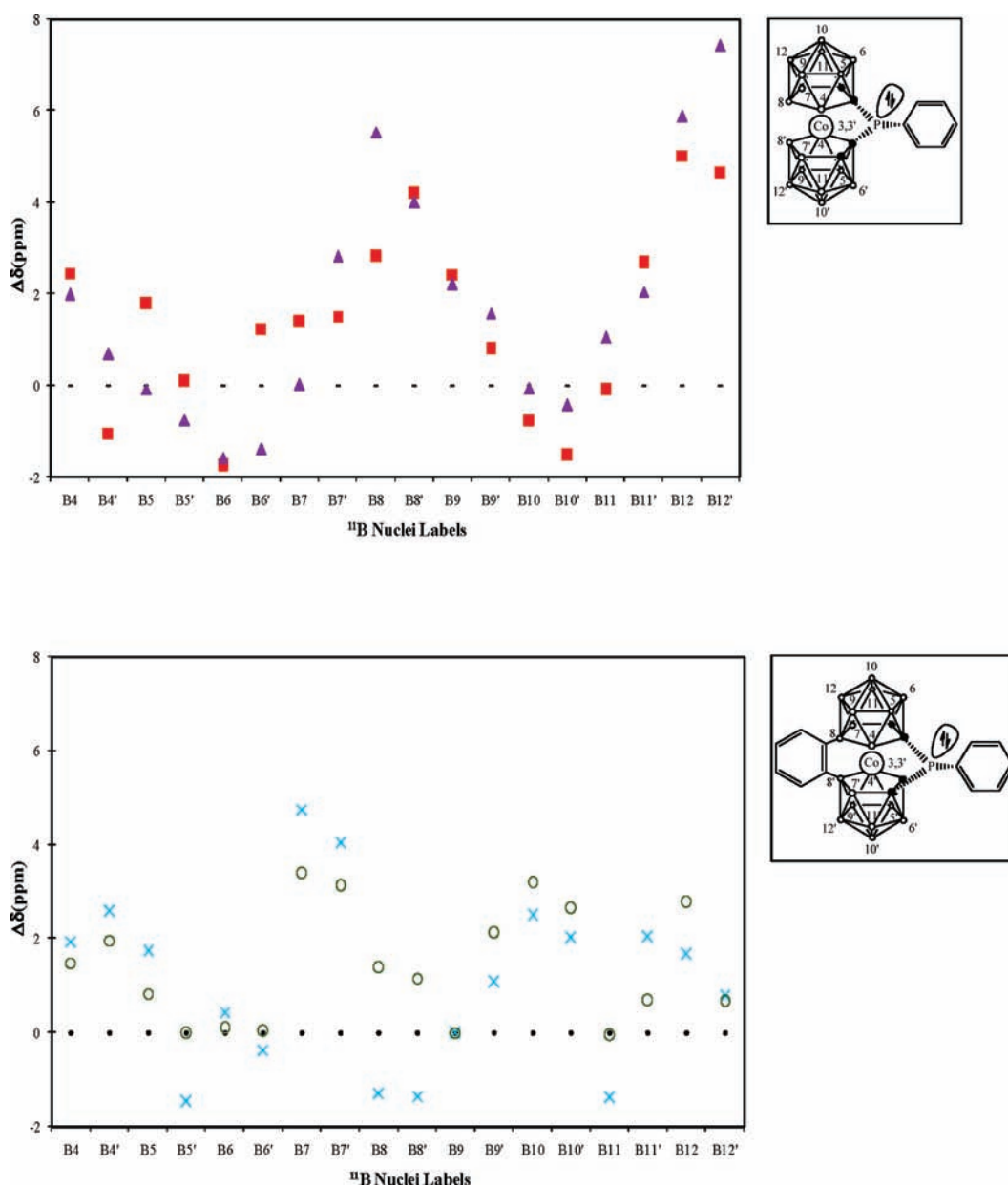


Figure 14. Plots of calculated ^{11}B NMR chemical shifts differences in $[3]^-$ (red \blacksquare) and $[4]^-$ (purple \blacktriangle) as referred to $[1]^-$: the dashed line at zero corresponds to the chemical shift in $[1]^-$; red \blacksquare and purple \blacktriangle correspond to $\delta([3]^-) - \delta([1]^-)$ and $\delta([4]^-) - \delta([1]^-)$, respectively. Plot at bottom corresponds to $[7]^-$ (blue \times) and $[8]^-$ (gray \circ) as referred to $[2]^-$ (pointed line).

original phospho[1]benzene[2]cobaltabisdicarbollidephane. In both oxidations, the $E_{1/2}(\text{Co}^{3+/2+})$ values shifted anodically, a precise 0.14 V for O, the shift being independent of R. Therefore, the lesser availability of the lone pair even accentuated the anodic shift attributed to the P. It remained to be studied if this anodic shift was a consequence of the opposing effect of the bridging benzene, or conversely, it was inherent to the bridging P-R moiety. To this aim, oxidation of phospho[1]cobaltabisdicarbollidephane, $[3]^-$, with H_2O_2 and sulfur, was conducted to yield compounds $[4]^-$ and $[5]^-$, respectively. The $E_{1/2}(\text{Co}^{3+/2+})$ value has experienced a 0.21 V anodic shift, slightly more accentuated than with the additional presence of the benzene bridge. This indicates that the additional anodic shift of the $\text{Co}^{3+/2+}$ couple is largely due to the lesser availability of the lone pair on P, but attenuated by the synergist effect of the confronting second ansa, 0.21 versus 0.14 V.

4. UV-Visible Spectrum. Hawthorne and co-workers^{2a} have reported that the UV-visible spectra of $[1]^-$ in methanol consists of four absorptions at 216, 293, 345, and 445 nm, which is grossly in agreement with this reported later by Matel and co-workers⁴⁴ with one absorption band (λ_{max} at 287 nm, $\epsilon \approx 30\,000 \text{ L} \cdot \text{cm}^{-1} \cdot \text{mol}^{-1}$). The visible spectrum was interpreted by Cerný and co-workers⁴⁵ on the basis of the Ligand Field Theory. We recorded the UV-visible spectra of $[1]^-$ in acetonitrile,^{8,11} as this is the solvent used in the cyclic voltammetry studies, and although the spectrum was rather similar to these already reported, discrepancies exist in the λ positions and the absorption coefficients which indicate that these values are dependent on how the absorption (A) was measured.

We have recorded the UV-visible spectrum of $[2]^-$, $[3]^-$, $[4]^-$, $[5]^-$, $[7]^-$, $[8]^-$, $[11]^-$, $[15]^-$, and $[16]^-$ in acetonitrile.

The spectra in general did not show well-defined peaks, which made it difficult to compare them. To overcome this problem, a deconvolution in Gaussian-type peaks was performed using line-fitting analysis. The goodness-of-fit (R^2) of all the spectra was between 0.999 and 0.996. The full set of data is shown in Table 9.

The results obtained for the parent compound $[1]^-$, as well as for the species $[3]^-$, $[4]^-$, and $[5]^-$, as representative examples are shown in Figure 15. As can be seen, the deconvolution in Gaussians permitted discernment of the sub-band positions and the retrieval of λ_{\max} that would otherwise have been impossible. Therefore, relevant comparisons can be made. It can be observed that absorptions near 220, 281, 329, and 445 nm, present in the spectrum of $[1]^-$, are indeed present in all the spectra with comparable λ values. These absorptions can then be attributed to the $[3,3'-\text{Co}(1,2-\text{C}_2\text{B}_9\text{H}_{11})_2]^-$ moiety. The benzene bridged cobaltabisdicarbollidephane, $[2]^-$, displays absorptions at 216, 236, 263, 275, 285, 297, 334, and 517 nm. These at 216, 285, 334, and 517 are almost coincident with the absorptions due to $[1]^-$. Therefore, the set of absorptions at 236, 263, and 275 nm can be ascribed to the benzene bridge as they are also observed in *o*-xylene.⁴⁶ These absorptions are present in all the remaining benzene bridged cobaltabisdicarbollidephanes. It is noteworthy that the absorption near 240 nm observed in $[7]^-$ and $[8]^-$ is not found in $[15]^-$ and $[16]^-$. The last two do not have the P-Ph moiety but the P^tBu, which would suggest that the $-PPh$ moiety

Table 8. Calculated NPA Charges on Cobalt, Cluster Total Charge (CTC), Energy Values (in eV) of the HOMO and LUMO Orbitals, Their Energy Difference, and Experimental $E_{1/2}$ [V/*fc*] for Several Monoansa and Diansa Metallacyclophanes

compound	NPA _{Co}	CTC	E_{HOMO}	E_{LUMO}	$\Delta(E_{\text{LUMO}} - E_{\text{HOMO}})$	$E_{1/2}$ [V]
$[1]^-$	-0.460	-3.031	-4.04	0.51	4.54	-1.80
$[2]^-$	-0.478	-2.384	-3.23	0.33	3.56	-2.11
$[3]^-$	0.314	-3.156	-3.93	0.37	4.30	-1.64
$[4]^-$	0.310	-3.219	-4.30	0.19	4.49	-1.43
$[5]^-$	0.307	-3.212	-	-	-	-1.47
$[6]^-$	0.306	-3.215	-	-	-	-
$[7]^-$	-0.646	-2.655	-3.32	0.30	3.63	-1.58
$[8]^-$	-0.660	-2.714	-3.46	0.14	3.60	-1.44
$[11]^-$	0.312	-3.200	-3.83	0.42	4.26	-1.66
$[15]^-$	-	-	-	-	-	-1.85
$[16]^-$	-	-	-	-	-	-1.71

also contributes, or in some cases is the only factor responsible for the absorptions near 240 nm. We have ruled out that the lone pair on P plays a role in this absorption as PR_3 ($R = \text{alkyl}$) do not absorb above 200 nm. The column headed by 329 nm in Table 9 does not contain any void. This suggests that this absorption can be assigned to the cobaltabisdicarbollide fragment; however, the two neighboring columns are complementary. The voids in the left column are filled in the right column, and vice versa. It is relevant to indicate that with no exception the compounds having absorptions near 370 nm are the diansa metallacyclophanes. Presumably,

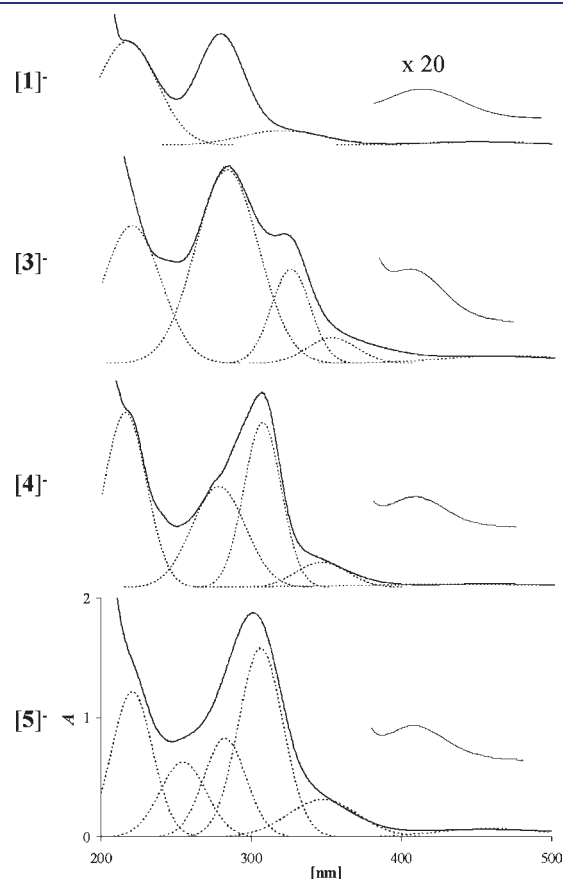


Figure 15. UV/vis spectra (solid lines) of some selected compounds, from top to bottom $[1]^-$, $[3]^-$, $[4]^-$, and $[5]^-$, and the results of line fitting with gaussians (dashed lines). The expanded sections on the right show the absorption near 450 nm amplified 20 times.

Table 9. UV-vis Spectra for Compounds $[1]^-$, $[2]^-$, $[3]^-$, $[4]^-$, $[5]^-$, $[7]^-$, $[8]^-$, $[11]^-$, $[15]^-$, and $[16]^-$ in Acetonitrile^a

compound	λ (ϵ)								
$[1]^{-38}$	220 (15.069)				281 (15.353)	329 (2.171)	445 (496)		
$[2]^-$	216 (21.571)	236 (13.429)	263 (5.857)	275 (6.286)	285 (12.540)	297 (14.143)	334 (3.403)	517 (586)	
$[3]^-$	221 (11.099)				284 (15.604)	327 (7.580)	354 (2.067)	461 (616)	
$[4]^-$	217 (12.702)				278 (7.337)	308 (11.958)	348 (1.835)	460 (252)	
$[5]^-$	222 (10.789)				283 (5.513)	308 (10.545)	349 (2.088)	456 (461)	
$[7]^-$	219 (11.223)	240 (8.399)	262 (4.061)	274 (4.271)	289 (6.623)		328 (2.736)	375 (950)	480 (415)
$[8]^-$	220 (11.682)	245 (3.689)	263 (3.976)		284 (8.722)	307 (15.693)	342 (2.354)	460 (220)	
$[11]^-$	210 (7.467)				287 (14.978)	312 (4.197)	340 (2.020)	459 (299)	
$[15]^-$	230 (10.853)		265 (3.899)	275 (3.248)	287 (9.670)		324 (3.812)	374 (973)	479 (583)
$[16]^-$	231 (10.910)		266 (4.176)	274 (4.078)	288 (11.138)		323 (3.730)	365 (1.339)	459 (457)

^aThe λ positions [nm] and ϵ values [$\text{L} \cdot \text{cm}^{-1} \cdot \text{mol}^{-1}$] are reported and were calculated following line-fitting analysis.

this band can be diagnosis for a synergistic effect between the two bridging units. In support of this is the difference of 20 nm in the column headed by 445 nm between the oxidized and nonoxidized phosphorus in $[7]^-/[8]^-$, and $[15]^-/[16]^-$, whereas this difference is not observed for the $[3]^-/[4]^-$ couple. Additionally, a change on the d–d band of around 20 nm is also observed for $[3]^-/[7]^-$, and $[11]^-/[15]^-$ that can be attributed to the inclusion of the second ansa moiety, the boron-bridged aromatic ring.

To interpret the former results, HOMO and LUMO orbitals for $[3]^-$, $[4]^-$, $[7]^-$, and $[8]^-$ have been compared. These frontier orbitals are shown in Figures 12 and 13. Some observations can be drawn from these figures; a straightforward one is that the contribution of phosphorus to the HOMO of $[3]^-$ is very important, while for $[4]^-$ it is nonexistent. This agrees with the results obtained both for the NBO analysis and the ^{31}P NMR. The delocalization of the HOMO between the P and the Co ensures an electronic communication between these atoms through the cluster C_c atoms, that also contribute to the HOMO. This data parallels the results of the NBO analysis. As expected for the oxidized phosphine, in $[4]^-$ the phosphorus does not contribute to the HOMO orbital, mostly constituted by a d orbital on cobalt. For diansa metallacyclophanes $[7]^-$ and $[8]^-$, the largest fragment contribution to the HOMO is due to the benzene bridging moiety; the lone pair in $[7]^-$ also contributes to the HOMO but its participation is much less than in $[3]^-$. No P contribution to the HOMO occurs in $[8]^-$. Of notice is the difference in $\Delta(E_{\text{LUMO}} - E_{\text{HOMO}})$ for monoansa $[3]^-$ and $[4]^-$ that is 0.19 eV and the diansa $[7]^-$ and $[8]^-$ that is 0.03 eV as can be deduced in Table 8. The smaller $\Delta\Delta(E_{\text{LUMO}} - E_{\text{HOMO}})$ for $[7]^-$ and $[8]^-$ has to be related to the synergistic effect of both ansa fragments discussed throughout the paper. The former values correlate with the electrochemical $E_{1/2}$ data shown in Table 8. While the $\Delta E_{1/2}([4]^-/[3]^-)$ is 0.21 V, the $\Delta E_{1/2}([8]^-/[7]^-)$ is 0.14 V. All LUMO orbitals are metal-centered and all look very similar. The LUMO energies of the mono and diansa are very similar, thus demonstrating that the synergistic effect or, more specifically, the lone pair influence is solely based on the HOMO orbitals.

The changes on the d–d transition band are related to the HOMO and LUMO energies that depend on the electronic environment around the metal center. The increasing ability to reduce the cobalt atom in moving from $[1]^-$ to $[3]^-$ to $[4]^-$ as a result of the donor ability of the phosphine ligand is, however, not observed as a shift of this band on these monoansa cobaltabisdicarbollidephanes. On the other hand, for diansa metallacyclophanes $[2]^-/[7]^-/[8]^-$, a blue shift is observed from 517 to 460 nm. This shift is also observed on the E_{LUMO} as this energy is related to the ease to reduce the metal center according to Koopman's theorem. In Table 8 can be seen a summary of E_{HOMO} , E_{LUMO} , and $\Delta E_{(\text{HOMO}-\text{LUMO})}$ for selected compounds. The effect of the substituent on the phosphorus atom (Ph or $t\text{Bu}$) is negligible on the UV-vis spectra and also on their orbital energies. When we look at the $\Delta E_{(\text{HOMO}-\text{LUMO})}$, we can observe the dramatic effect of the aromatic B-bridge unit as it lowers the energy difference 1 eV. On the contrary, the donor ability of the phosphine ligand is observed on the E_{LUMO} which decreases as it goes from $[1]^-$ to $[3]^-$ and $[4]^-$, and also from $[2]^-$ to $[7]^-$ and $[8]^-$.

CONCLUSIONS

The first highly compact diansa metallacyclophane has been prepared in which the two ansa units are not adjacent. The central core is the sandwich $[\text{Co}(\text{C}_2\text{B}_9\text{H}_{11})_2]^-$ and two rigid nonadjacent

handles, one single P and two adjacent carbon atoms of a benzene ring, complete the molecule that has the shape of an amphora. The different nature of the two handles, geometrically placed in a confronting disposition, results in a donor and acceptor system with a redox electroactive core. The synergy of the two handles is reflected in every aspect of the molecule, including structure, electronic and spectroscopic properties, and redox activity. For instance, the confronted disposition of the two handles permits the two “ C_2B_3 ” cobalt coordinating planes to be quasi parallel, with almost no distortion relative to the pristine $[\text{Co}(\text{C}_2\text{B}_9\text{H}_{11})_2]^-$. Contrarily, a noticeable deviation from the latter is found with the monoansa either phosphane $[3]^-$ or benzene precursor $[2]^-$. Another example of the synergy of the two handles is found in the redox activity of the $\text{Co}^{3+/2+}$ couple: the combined effect of the two handles shifts the $E_{1/2}$ to an E -value that is not the simple addition of the two individual effects: one of them is clearly enhanced. Very important is the role of the phosphorus lone pair. When available, the lone pair does participate in the electronic communication between the two handles through the redox electroactive site. This communication is blocked when the phosphorus lone pair is used for other activities outside the amphora molecule, for example, when it is used to generate a P–E bond, $E = \text{O}, \text{S}, \text{or Se}$. We expect that the geometrical, electronic, and electrochemical properties of these robust and compact amphora-like diansa molecules will contribute to the generation of a new set of molecular functional materials for applications in molecular electronics, sensors, and light harvesting, among others.

ASSOCIATED CONTENT

S Supporting Information. An experimental section with full characterization of the synthesized compounds, crystallographic data [the crystallographic data for tetramethylammonium salts of compounds $[4]^-$ – $[7]^-$ can be obtained free of charge via www.ccdc.cam.ac.uk/conts/retrieving.html (or from the Cambridge Crystallographic Data Centre, 12 Union Road, Cambridge CB2 1EZ, U.K.; fax (+44) 1223-336033; or e-mail deposit@ccdc.cam.ac.uk)], and calculation details; MALDI-TOF-MS of $[\text{NMe}_4][3]$ and $[\text{NMe}_4][6]$ (Figure S1); plots of calculated ^{11}B NMR diamagnetic (Figure S2) and paramagnetic (Figure S3) shielding constant differences in $[3]^-$ and $[4]^-$ as well as $[7]^-$ and $[8]^-$ referred to $[1]^-$ and $[2]^-$, respectively; second-order delocalization energies for the electron lone pairs and NBOs antibonding interactions for some monoansa and diansa phosphacobaltabisdicarbollidephanes (Table S1). This material is available free of charge via the Internet at <http://pubs.acs.org>.

AUTHOR INFORMATION

Corresponding Author

clara@icmab.es

ACKNOWLEDGMENT

This work was supported by Spanish Ministerio de Ciencia e Innovación (CTQ2010-16237), CSIC (I3P grant to P.F.) and the Generalitat de Catalunya 2009/SGR/00279. The access to the computational facilities of High Performance Computing Centre of CSIC and Centre de Serveis Científics i Acadèmics de Catalunya (CESCA) is gratefully acknowledged. P.G.-C. enrolled in the UAB PhD program.

REFERENCES

- (1) (a) Hawthorne, M. F.; Young, D. C.; Wegner, P. A. *J. Am. Chem. Soc.* **1965**, *87*, 1818. (b) Hawthorne, M. F.; Andrews, T. D. *Chem. Commun.* **1965**, 443.
- (2) (a) Hawthorne, M. F.; Young, D. C.; Andrews, T. D.; Hove, D. V.; Pilling, R. L.; Pitts, A. D.; Reinjes, M.; Warren, L. F.; Wegner, P. A. *J. Am. Chem. Soc.* **1968**, *90*, 879. (b) Mingos, D. M. P. *J. Chem. Soc., Dalton Trans.* **1977**, 602.
- (3) Grabulosa, A. *P-Stereogenic Ligands in Enantioselective Catalysis*; RSC Catalysis Series; Royal Society of Chemistry: Cambridge, 2011.
- (4) Rinehart, A. K., Jr.; Frerichs, P. A.; Kittle, L. F.; Westmann, L. F.; Gustafson, R. L.; Pruett, J. E.; McMahon, J. E. *J. Am. Chem. Soc.* **1960**, *82*, 4111.
- (5) Osborne, A. G.; Whiteley, R. H. *J. Organomet. Chem.* **1975**, *101*, C27.
- (6) For a recent review see: Herbert, D. E.; Mayer, U. F. J.; Manners, I. *Angew. Chem., Int. Ed.* **2007**, *46*, 5060.
- (7) Brandt, P. F.; Compton, D. L.; Rauchfuss, T. B. *Organometallics* **1998**, *17*, 2702.
- (8) Rojo, I.; Teixidor, F.; Viñas, C.; Kivekäs, R.; Sillanpää, R. *Chem.—Eur. J.* **2003**, *9*, 4311.
- (9) Connelly, N. G.; Geiger, W. E. *Chem. Rev.* **1996**, *96*, 877.
- (10) Sivaev, I. B.; Bregadze, V. I. *Collect. Czech. Chem. Commun.* **1999**, *64*, 783.
- (11) (a) Chamberlin, R. M.; Scott, B. L.; Melo, M. M.; Abney, K. D. *Inorg. Chem.* **1997**, *36*, 809. (b) Juárez-Pérez, E. J.; Viñas, C.; González-Campo, A.; Teixidor, F.; Sillanpää, R.; Kivekäs, R.; Núñez, R. *Chem.—Eur. J.* **2008**, *14*, 4924.
- (12) (a) Viñas, C.; Pedrajas, J.; Bertran, J.; Teixidor, F.; Kivekäs, R.; Sillanpää, R. *Inorg. Chem.* **1997**, *36*, 2482. (b) Viñas, C.; Gomez, S.; Bertran, J.; Teixidor, F.; Dozol, J. F.; Rouquette, H. *Chem. Commun.* **1998**, 191. (c) Viñas, C.; Gomez, S.; Bertran, J.; Teixidor, F.; Dozol, J. F.; Rouquette, H. *Inorg. Chem.* **1998**, *37*, 3640. (d) Viñas, C.; Bertran, J.; Gomez, S.; Teixidor, F.; Dozol, J. F.; Rouquette, H.; Kivekäs, R.; Sillanpää, R. *J. Chem. Soc., Dalton Trans.* **1998**, 2849. (e) Viñas, C.; Pedrajas, J.; Teixidor, F.; Kivekäs, R.; Sillanpää, R.; Welch, A. J. *Inorg. Chem.* **1997**, *36*, 2988.
- (13) (a) Francis, J. N.; Hawthorne, M. F. *Inorg. Chem.* **1971**, *10*, 594. (b) Shelly, K.; Knobler, C. B.; Hawthorne, M. F. *New J. Chem.* **1988**, 317.
- (14) (a) Mortimer, M. D.; Knobler, C. B.; Hawthorne, M. F. *Inorg. Chem.* **1996**, *35*, 5750. (b) Rojo, I.; Teixidor, F.; Kivekäs, R.; Sillanpää, R.; Viñas, C. *Organometallics* **2003**, *22*, 4642. (c) Beletskaya, I. P.; Bregadze, V. I.; Ivushkin, V. A.; Petrovskii, P. V.; Sivaev, I. B.; Sjöberg, S.; Zhigareva, G. G. *J. Organomet. Chem.* **2004**, *689*, 2920.
- (15) Farràs, P.; Olid-Britos, D.; Viñas, F.; Teixidor, F. *Eur. J. Inorg. Chem.* **2011**, 2525.
- (16) (a) Plešek, J.; Hermánek, S.; Base, K.; Todd, L. J.; Wright, W. F. *Collect. Czech. Chem. Commun.* **1976**, *41*, 3509. (b) González-Cardoso, P.; Stoica, A.-I.; Farràs, P.; Pepiol, A.; Viñas, C.; Teixidor, F. *Chem.—Eur. J.* **2010**, *16*, 6660.
- (17) (a) Teixidor, F.; Viñas, C.; Abad, M. M.; Kivekäs, R.; Sillanpää, R. *J. Organomet. Chem.* **1996**, *509*, 139. (b) Viñas, C.; Núñez, R.; Teixidor, F.; Sillanpää, R.; Kivekäs, R. *Organometallics* **1999**, *18*, 4717.
- (18) Verkade, J. G.; Mosbo, J. A. In *Phosphorus-31 NMR Spectroscopy in Stereochemical Analysis*; Quin, L. D., Verkade, J. G., Eds.; VCH: New York, 1987; pp 425–463.
- (19) McFarlane, W.; Rycroft, D. S. *J. Chem. Soc., Dalton Trans.* **1973**, *20*, 2162.
- (20) Allen, D. W.; Taylor, B. F. *J. Chem. Soc., Dalton Trans.* **1982**, *1*, 51.
- (21) Jameson, C. J. In *Phosphorus-31 NMR Spectroscopy in Stereochemical Analysis*; Quin, L. D., Verkade, J. G., Eds.; VCH: New York, 1987; pp 205–230.
- (22) Klapötke, T. M.; Broschag, M. *Compilation of Reported 77Se NMR Chemical Shifts*; Wiley: Chichester, 1996.
- (23) Burford, N.; Royan, B. W.; Spence, R. E. v. H.; Rogers, R. D. *Dalton Trans.* **1990**, 7, 2111.
- (24) Pyykkö, P.; Atsumi, M. *Chem.—Eur. J.* **2009**, *15*, 12770.
- (25) (a) Stoeckli-Evans, H.; Osborne, A. G.; Whiteley, R. H. *J. Organomet. Chem.* **1980**, *194*, 91. (b) Butler, I. R.; Cullenm, W. R.; Einstein, F. W. B.; Rettig, S. J.; Willis, A. J. *Organometallics* **1983**, *2*, 128.
- (26) Patra, S. K.; Whittell, G. R.; Nagiah, S.; Ho, C.-L.; Wong, W.-Y.; Manners, I. *Chem.—Eur. J.* **2010**, *16*, 3240.
- (27) Rojo, I.; Teixidor, F.; Kivekäs, R.; Sillanpää, R.; Viñas, C. *J. Am. Chem. Soc.* **2003**, *125*, 14720.
- (28) Cook, J. B.; Nicholson, B. K.; Smith, D. W. *J. Organomet. Chem.* **2004**, *689*, 860 and references therein.
- (29) Popescu, A. R.; Laromaine, A.; Teixidor, F.; Sillanpää, R.; Kivekäs, R.; Llambias, J. I.; Viñas, C. *Chem.—Eur. J.* **2011**, *17*, 4429.
- (30) Allen, F. H. *Acta Crystallogr.* **2002**, *B58*, 380.
- (31) CSD codes AMCOCB10, AMCOCB, CAKXOC, GOCBEF, IQAKIV, GOPNOO, RULMOA, WUJZUW, and WUJZOQ.
- (32) Bondi, A. J. *Phys. Chem.* **1964**, *68*, 441.
- (33) Bader, R. F. W. *Atoms in Molecules: A Quantum Theory*; Clarendon Press: Oxford, New York, 1990.
- (34) Todd, L. J.; Siedle, A. R. *Prog NMR Spectrosc.* **1979**, *13*, 87.
- (35) (a) Grimes, R. N. *Carboranes*, 2nd ed.; Elsevier: New York/Oxford, 2011. (b) Hermanek, S.; Plešek, J.; Stibr, B.; Grigor, V. *J. Chem. Soc., Chem. Commun.* **1977**, 561. (c) Stanko, V. I.; Babushkina, T. A.; Klimova, T. P.; Golytshin, Y. U.; Klimova, A. I.; Vasilev, A. M.; Alymov, A. M.; Khrapov, V. V. *Zh. Obshch. Khim.* **1976**, *46*, 1071. (d) Teixidor, F.; Viñas, C.; Rudolph, R. W. *Inorg. Chem.* **1986**, *25*, 3339.
- (36) (a) Bühl, M.; Hnyk, D.; Macháček, J. *Chem.—Eur. J.* **2005**, *11*, 4109. (b) Pennanen, T. O.; Macháček, J.; Taubert, S.; Vaara, J.; Hynk, D. *Phys. Chem. Chem. Phys.* **2010**, *12*, 7018.
- (37) Parish, R. V. *NMR, NQR, EPR, and Mössbauer spectroscopy in Inorganic Chemistry*; Ellis Horwood Series in Inorganic Chemistry. J. Burgess, Ed.; Ellis Horwood Limited: West Sussex, England, 1990.
- (38) Rojo, I.; Teixidor, F.; Viñas, C.; Kivekäs, R.; Sillanpää, R. *Chem.—Eur. J.* **2004**, *10*, 5376.
- (39) (a) Teixidor, F.; Núñez, R.; Viñas, C.; Sillanpää, R.; Kivekäs, R. *Angew. Chem., Int. Ed.* **2000**, *39*, 4290. (b) Núñez, R.; Farràs, P.; Teixidor, F.; Viñas, C.; Sillanpää, R.; Kivekäs, R. *Angew. Chem., Int. Ed.* **2006**, *45*, 1270. (c) Teixidor, F.; Núñez, R.; Viñas, C.; Kivekäs, R.; Sillanpää, R. *Inorg. Chem.* **2001**, *40*, 2587.
- (40) Manners, I. Ring-Opening Polymerization of Metallocenophanes: A New Route to Transition Metal-Based Polymers; *Advances in Organometallic Chemistry*, Vol. 37; Academic Press: New York, 1995.
- (41) Pudelski, J. K.; Foucher, D. A.; Honeyman, C. H.; Lough, A. J.; Manners, I.; Barlow, S.; O'Hare, D. *Organometallics* **1995**, *14*, 2470.
- (42) Oliva, J. M.; Viñas, C. *J. Mol. Struct.* **2000**, *556*, 33.
- (43) (a) Lever, A. B. P. *Inorg. Chem.* **1990**, *29*, 1271. (b) Lever, A. B. P. *Inorg. Chem.* **1991**, *30*, 1980. (c) Lever, A. B. P.; Dodsworth, E. S. *Inorganic Electronic Structure and Spectroscopy*; Solomon, E. I., Lever, A. B. P., Eds.; Wiley: New York, 1999; Vol. 2, pp 227–287.
- (44) Matel, L.; Macásek, F.; Rajec, P.; Hermánek, S.; Plešek, J. *Polyhedron* **1982**, *1*, 511.
- (45) Cerný, V.; Pavlík, I.; Kustková-Maxová, E. *Collect. Czech. Chem. Commun.* **1976**, *41*, 3232.
- (46) Fally, S.; Carleer, M.; Vandaele, A. C. *J. Quant. Spectrosc. Radiat. Transfer* **2009**, *110*, 766.
- (47) Juárez-Pérez, E. J.; Núñez, R.; Viñas, C.; Sillanpää, R.; Teixidor, F. *Eur. J. Inorg. Chem.* **2010**, 2385.